Structure

Article

Structural requirements for the specific binding of CRABP2 to cyclin D3

Graphical abstract

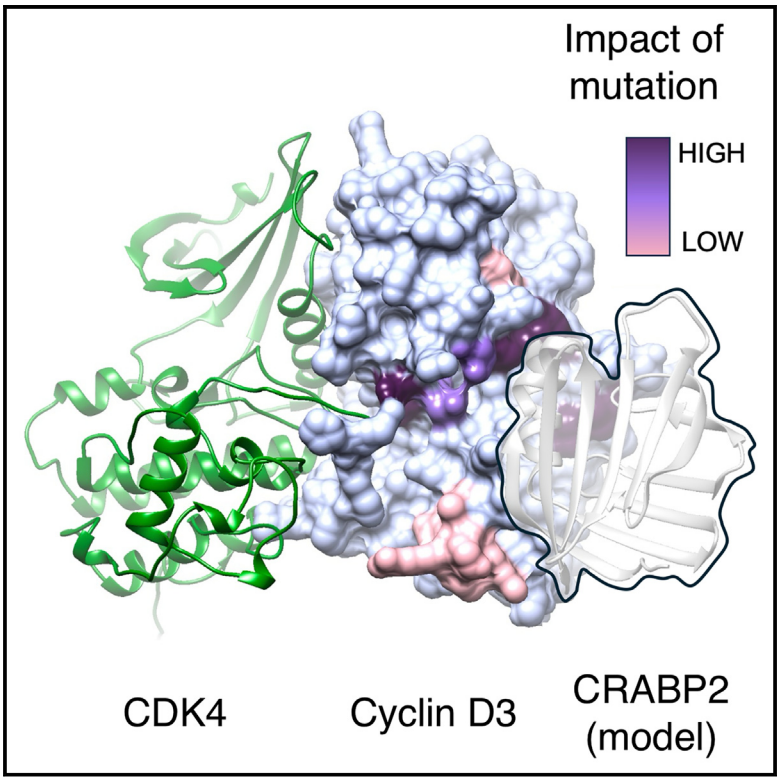

Highlights

- CRABP2 binds selectively to CDK4/6-cyclin D3 and not to CDK4/6 or CDK4/6-cyclin D1
- The CRABP2 nuclear localization sequence and cyclin D3 binding site overlap
- CRABP2 mutants adopt alternative monomeric CRABP2 conformations
- Cyclin D3 mutants identify a protein binding site on the C-terminal cyclin box fold

Authors

Martyna W. Pastok, Charles W.E. Tomlinson, Shannon Turberville, ..., Jane A. Endicott, Ehmke Pohl, Natalie J. Tatum

Correspondence

martyna.pastok@gmail.com (M.W.P.), jane.endicott@newcastle.ac.uk (J.A.E.), natalie.tatum@newcastle.ac.uk (N.J.T.)

In brief

Using purified proteins, Pastok et al. confirm CRABP2 binding to cyclin D3. Their mutational study, supported by crystal structures of CRABP2 mutants and AlphaFold modeling, identifies a protein-protein interaction interface between the cyclin D3 C-terminal cyclin box fold and the CRABP2 helical cap.

Pastok et al., 2024, Structure *32*, 1–15
December 5, 2024
https://doi.org/10.1016/j.str.2024.09.020

CellPress

Please cite this article in press as: Pastok et al., Structural requirements for the specific binding of CRABP2 to cyclin D3, Structure (2024), https://doi.org/10.1016/j.str.2024.09.020

Structure

CellPress
OPEN ACCESS

Article

Structural requirements for the specific binding of CRABP2 to cyclin D3

Martyna W. Pastok,[1,5,*] Charles W.E. Tomlinson,[2,6] Shannon Turberville,[1] Abbey M. Butler,[2] Arnaud Baslé,[3] Martin E.M. Noble,[1] Jane A. Endicott,[1,7,*] Ehmke Pohl,[2,4] and Natalie J. Tatum[1,*]

[1]Newcastle University Centre for Cancer, Translational and Clinical Research Institute, Newcastle University, Paul O'Gorman Building, Framlington Place, Newcastle upon Tyne NE2 4HH, UK
[2]Department of Chemistry, Durham University, Lower Mountjoy, South Road, Durham DH1 3LE, UK
[3]Biosciences Institute, Newcastle University, Framlington Place, Newcastle upon Tyne NE2 4HH, UK
[4]Department of Biosciences, Durham University, Upper Mountjoy, South Road, Durham DH1 3LE, UK
[5]Present address: Captor Therapeutics S.A., Duńska 11, 54-427 Wrocław, Poland
[6]Present address: Department of Biology, York University, York YO10 5DD, UK
[7]Lead contact
*Correspondence: martyna.pastok@gmail.com (M.W.P.), jane.endicott@newcastle.ac.uk (J.A.E.), natalie.tatum@newcastle.ac.uk (N.J.T.)
https://doi.org/10.1016/j.str.2024.09.020

SUMMARY

Cellular retinoic acid binding protein 2 (CRABP2) transports retinoic acid from the cytoplasm to the nucleus where it then transfers its cargo to retinoic acid receptor-containing complexes leading to activation of gene transcription. We demonstrate using purified proteins that CRABP2 is also a cyclin D3-specific binding protein and that the CRABP2 cyclin D3 binding site and the proposed CRABP2 nuclear localization sequence overlap. Both sequences are within the helix-loop-helix motif that forms a lid to the retinoic acid binding pocket. Mutations within this sequence that block both cyclin D3 and retinoic acid binding promote formation of a CRABP2 structure in which the retinoic acid binding pocket is occupied by an alternative lid conformation. Structural and functional analysis of CRABP2 and cyclin D3 mutants combined with AlphaFold models of the ternary CDK4/6-cyclin D3-CRABP2 complex supports the identification of an α-helical protein binding site on the cyclin D3 C-terminal cyclin box fold.

INTRODUCTION

Members of the intracellular lipid-binding protein (iLBP) family sequester and transport a diverse array of lipophilic molecules between organs and intracellular compartments with differing affinities and selectivity.[1–3] They are diverse in primary sequence, but highly conserved in structure, sharing a β-barrel fold formed by two five-stranded β sheets that generates a large and deep binding cavity for the lipophilic cargo.[4] A helix-loop-helix motif (α1-loop-α2) caps and occludes the cavity effectively solubilizing the ligand within a protein shell.[5–7]

CRABP2 (cellular retinoic acid binding protein 2) is a small (15.7 kDa) highly conserved protein that belongs to the family of retinoic acid (RA) binding proteins that also includes CRABP1 and CRBPI-IV. It binds *all-trans*, 9-*cis*, and 13-*cis* RA with nanomolar affinity,[8] and its primary function is to shuttle its cargo from the cytoplasm to the nucleus,[9] where it binds specifically to the retinoic acid receptor (RAR); retinoid-X-receptor (RXR) heterodimer.[10] Subsequent transfer of RA from CRABP2 to the receptor complex activates programs of coordinated gene transcription.[9,10] Dependent on context, RAR-RXR can promote differentiation, apoptosis, and cell-cycle arrest.[11–13] Within the cytoplasm, a second function of apo-CRABP2 is to bind and stabilize the RNA binding protein HuR, and through it enhance the stability and expression of HuR-dependent transcripts.[14] Binding of RA and HuR to CRABP2 is mutually exclusive and both activities are thought to contribute to CRABP2's ability to act as a tumor suppressor. However, taken together other studies do not come to a consensus and suggest conflicting roles for CRABP2 in tumorigenesis executed by both RA-dependent and -independent activity and dependent on cell type.[15–19]

CRABP1 shares a high sequence identity (77%) with CRABP2 but is localized entirely into the cytoplasm, where it buffers retinoid concentrations within the cell, aiding in the degradation of retinoids via cytochrome P450.[20] In addition, CRABP1 can modulate several putative non-genomic pathways. The ERK1/2 kinase pathway is dose dependently modified by the CRABP1-all *trans* retinoic acid (ATRA) complex via sequential interactions with Raf, Mek, and Erk proteins,[21,22] and the calmodulin-dependant protein kinase pathway is modified by reduced autophosphorylation of CaMKII in the presence of CRABP1.[23] Deficiency or excess of vitamin A (of which RA is the carboxylic acid form) leads to severe developmental defects underscoring the importance of RA homeostasis and the appropriate regulation of its distribution and activity by CRABP1/2.[24,25]

Please cite this article in press as: Pastok et al., Structural requirements for the specific binding of CRABP2 to cyclin D3, Structure (2024), https://doi.org/10.1016/j.str.2024.09.020

Retinoids bind to CRABP1/2 in the hydrophobic pocket. At the base of the pocket are three conserved residues (R112, R132, Y134, and R112, R133 and Y135 in CRABP1 and CRABP2, respectively) that coordinate the ATRA acid group, usually in concert with a water molecule conserved in all structures with similarly binding ligands.[26] The rest of the pocket is lined with hydrophobic residues that create a suitable environment for the unsaturated, fatty-acid-like portion of ATRA. The cavity is quite large for such a small protein and in the absence of ligand, a series of water-mediated interactions within the cavity have been proposed to maintain the integrity of the fold.[27] Indeed, a comparison of the crystal structures of apo- (PDB 2FS6 [28]) and holo-CRABP2 (PDB 1CBS [26]) reveals there is little difference (root-mean-square deviation [RMSD] 1.1 Å over all 137 Cα pairs) between them.[28]

The molecular mechanisms by which CRABP2 binds RA, transports it through the nuclear membrane, and then channels its cargo to the receptor have not been fully elaborated. Comparative analysis of authentic apo- and ligand bound iLBP structures has suggested that given their similarities both ligand uptake and release must be accompanied by significant conformational change. A model for RA uptake was proposed from a comparison of the structures of CRABP2 bound to ATRA and an R112 mutant.[5] In the latter structure, significant concerted re-arrangements in the α2 helix which appears flexible and partially unwound, and the βC-βD and βE-βF hairpin loops generated a conformation that would permit RA access. The solution structure determined by NMR also revealed a more open entrance compatible with ligand entry.[29]

RA binding to apo-CRABP2 leads to the concomitant exposure of a non-canonical nuclear localization signal (NLS) which is not present in CRABP1.[30] This signal is not immediately recognizable as a consensus NLS sequence but instead adopts a tertiary structure that locates residues K21 (within α1), and R30 and K31 (located in α2) to resemble a classical NLS.[31] As such it is hypothesized to be recognized by importin-α, to transport CRABP2-RA across the nuclear pore complex. In support of this model, this non-classical NLS is conserved in other members of the iLBP family, in FABP4[32] and in FABP5 in response to binding of a subset of fatty acids that stimulate PPAR β/δ activity.[33] The bound RA is then proposed to be "channeled" from CRABP2 to the RAR through appropriate juxtaposition of their RA binding sites,[8] but the mechanism is yet to be elucidated.[34]

Other interactions between CRABP2 and its protein partners have been mapped that taken together provide further evidence that the structural elements that form the entrance to the cavity are a focal point for CRABP2 regulation. Despite the high sequence identity between CRABP2 and CRABP1, CRABP1 does not bind to the RAR.[35] Reciprocal mutations to CRABP1 and CRABP2 by swapping the identities of residues at CRABP2 positions 75 and 81 located on the βE-βF loop and facing the α1-loop-α2 cap across the mouth of the cavity, and at residue 102 within the βG-βH loop revealed the importance of this surface for CRABP2-RAR interaction.[34] CRABP2 mutated to the equivalent residues in CRABP1 (Q75E, P81K, and K102E) showed diminished ability to enhance RAR-dependent gene transcription, whereas the CRABP2-ised CRABP1 could now activate RAR. However, mutation of the CRABP2 NLS by replacing K21, R30, and K31 with alanine does not affect its binding to HuR suggesting that this protein interface is distinct.[14]

CRABP2 was identified as a cyclin D3 binding protein following a yeast-two-hybrid screen using a hematopoietic HL60 cDNA library.[36] Cyclin D3 was subsequently shown to enhance RA-mediated transactivation of RA target genes by interaction with both CRABP2 and the RAR. Cyclin D3 binding to CRABP2 was shown to be RA independent. However, cyclin D3 association with the RAR required RA. Importantly cyclin D1 and cyclin D2 did not share these functions with cyclin D3 suggesting a cyclin D3-specific role in RA signaling.[36]

The D-type cyclins are expressed in response to mitogenic growth factor signals early in G1 phase of the cell cycle and collectively are cognate partners for CDK4 and CDK6.[37,38] CDK4/6-cyclin D-dependent phosphorylation of the retinoblastoma protein pRB leads to the relief of inhibition of the E2F transcription factor and the expression of proteins required for G1 progression[39] Beyond cell cycle control, CDK4 and CDK6 and the three D-type cyclins function independently or in complexes within different cell-type specific molecular assemblies to regulate other aspects of cell behavior, such as transcription factor driven programmes,[40] cell metabolism,[41–43] differentiation,[44,45] and DNA repair.[46–48] Studies with cyclin D knockout mice have demonstrated both their functional diversity outside of cell cycle control and their abilities to compensate for each other in different cell lineages.[49,50] Notably, one cyclin D isoform is sufficient for cell cycle progression, but at least two are required for mouse survival.

We have reconstituted the CDK4/6-cyclin D3-CRABP2 complex and confirm that CRABP2 binds to cyclin D3 but not to cyclins D1 or D2 and that this CRABP2 activity is not shared with CRABP1. By high-resolution crystal structure determination and functional characterization of CRABP2 mutants, we identify the cyclin D3 binding site on CRABP2 and show that cyclin D3 binding is dependent upon the conformation of the NLS. CRABP2 association with retinoic acid does not change its affinity for cyclin D3 nor do CRABP2 mutations within the pocket that prevent RA association. The cyclin D3 binding site on CRABP2 is distinct from the RAR and HuR binding sites mapped by mutagenesis studies.

Employing AlphaFold2 Multimer,[51] we have generated a model of the ternary CDK4-cyclin D3-CRABP2 complex and validated it by CRABP2 and cyclin D3 mutation. This model identifies an α-helical protein binding site on cyclin D3 distinct from the CDK interface and the previously characterized cyclin recruitment site. It extends the cyclin D surface engaged in protein-protein interactions to include the C-terminal cyclin box fold (C-CBF).

RESULTS

CRABP2 is a cyclin D3-specific binding protein

CRABP2 has been shown to interact with cyclin D3 in a yeast two hybrid cell-based assay.[36] To confirm that the interaction is direct and specific for cyclin D3, we prepared recombinant monomeric CDK4 and CDK6, and CDK4/6- cyclin D1 and cyclin D3 complexes and assessed their interaction with CRABP2 using an established homogeneous time-resolved fluorescence (HTRF) assay[52] (Figures 1A and 1B). Using this assay CRABP2 interacts

Please cite this article in press as: Pastok et al., Structural requirements for the specific binding of CRABP2 to cyclin D3, Structure (2024), https://doi.org/10.1016/j.str.2024.09.020

CellPress
OPEN ACCESS

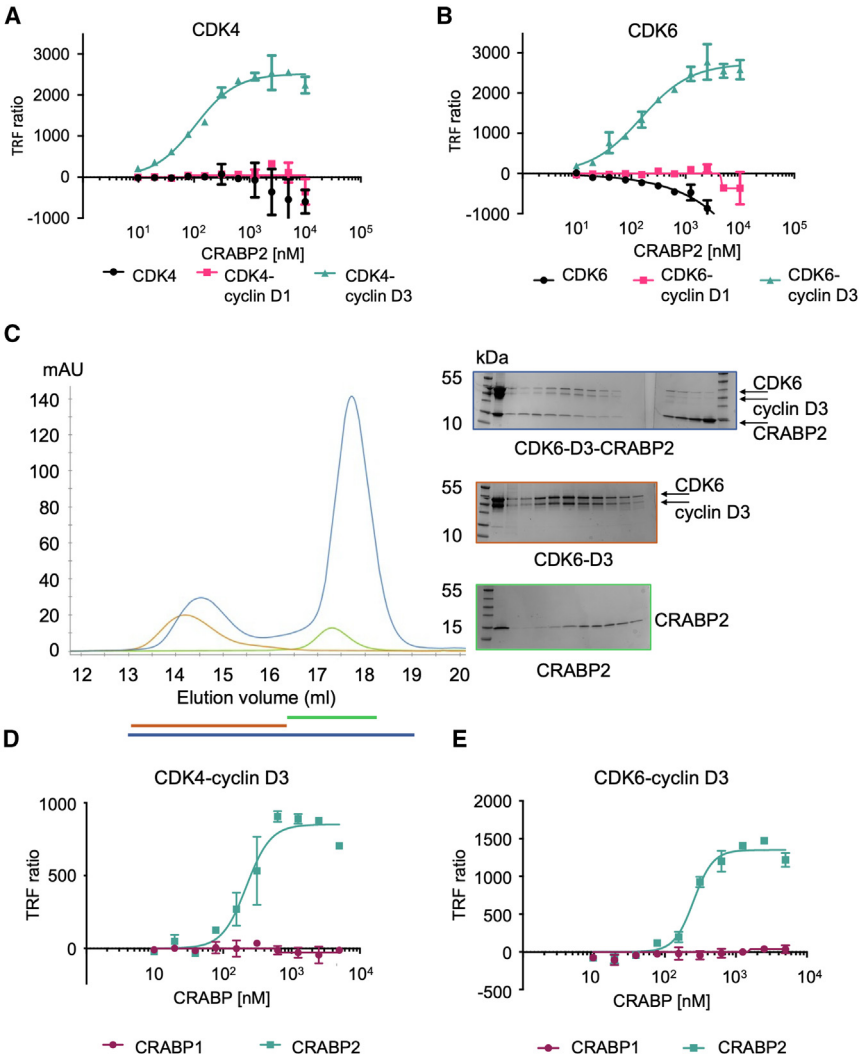

Figure 1. CRABP2 binds to cyclin D3

(A and B) CRABP2 binding to CDK4-cyclin D3 (A) or CDK6-cyclin D3 (B) (green curves) as measured by homogeneous time-resolved fluorescence (HTRF). CRABP2 does not bind to monomeric CDK4 or CDK6 (pink curves) or to CDK4/6-cyclin D1 complexes (black curves).

(C) Analytical size-exclusion chromatography. CRABP2 forms a stable complex with CDK6-cyclin D3 (blue trace). CDK6-cyclin D3 (brown) and CRABP2 (green) traces are overlaid to compare mobility. Lines underneath the chromatograms identify the elution ranges analyzed by SDS-PAGE shown in the panels on the right. Molecular weight markers, 10, 15, 25, 35, 40, and 55 kDa. Samples were visualized by Instant Blue staining. Chromatogram is representative of two replicates carried out using independently prepared proteins. Representative uncropped gels are presented in Figure S1A.

(D and E) CRABP1 does not bind to cyclin D3. CRABP1 and CRABP2 were titrated against CDK4-cyclin D3 (D) and CDK6-cyclin D3 (E). The concentration of CDK4, CDK4-cyclin D3, CDK6 and CDK6-cyclin D3 in the HTRF assays is 10 nM CRABP2 or CRABP1 was titrated in 2-fold dilutions starting at 10 μM. HTRF measurements were carried out in duplicate and repeated on 3 separate days. The error bars indicate SD.

with CDK4-cyclin D3 (K_d = 118 ± 49 nM) and CDK6-cyclin D3 (K_d = 113 ± 60 nM) with very similar affinities and does not interact with monomeric CDK4 or CDK6 or CDK4/6-cyclin D1 complexes (Table 1). To confirm the cyclin D3-CRABP2 interaction by an orthogonal technique, we carried out size-exclusion chromatography (Figures 1C and S1A). CRABP2 elutes as a monomer in the absence of CDK6-cyclin D3 but in its presence forms a ternary complex that elutes slightly later than CDK6-cyclin D3. This mobility pattern both confirms that CRABP2 binds to CDK6-cyclin D3 and suggests that binding is accompanied by a compacting of the CDK6-cyclin D3 structure evidenced by the decreased mobility of the complex despite its increase in size.

CRABP2 buries RA within a deep hydrophobic pocket occluding it from solvent. To determine whether cyclin D3 association is compatible with RA binding, we first prepared a series of CRABP2-RA derivative complexes and then compared their abilities to bind to CDK4-cyclin D3 and CDK6-cyclin D3 by HTRF (Figures S1B and S1C). The RA derivatives bind to CRABP2 with nM affinities (Table S1) so that a substantial proportion of the CRABP2 remains in the ligand-bound form during the titration. As measured by HTRF, the affinity of CRABP2 for cyclin D3 is not affected by the presence of bound RA or derivatives. To confirm this observation, we next assembled ternary CDK4- and CDK6-cyclin D3-CRABP2 complexes and incubated them on ice for 60 min in the presence of RA (Figures S1D and S1E). Increasing concentrations of RA or its derivatives did not result in cyclin D3-CRABP2 dissociation, as evidenced by an inability to inhibit the HTRF signal. At the final titration point, the RA derivative was in 10-fold excess of its CRABP2 K_d and present at 10-fold molar excess over CDK4/6-cyclin D3-CRABP2.

Finally, using the same HTRF assay format, we demonstrated that CRABP1 does not interact with cyclin D3 (Figures 1D and 1E). Taken together these results confirm that CRABP2 binds specifically to cyclin D3 and that this function is not shared with its close homolog CRABP1. Cyclin D3 binding to CRABP2 is RA independent.

CRABP2 mutations map residues required for cyclin D3 binding to the nuclear localization signal

To identify the cyclin D3 binding site on CRABP2, we first prepared a set of mutants at known CRABP2 protein and RA interaction sites (Figures 2A and 2B). The CRABP2 triple mutant Q75E/P81K/K102E incorporates amino acid differences between CRABP2 and CRABP1 and does not bind to the RAR.[34] Q75, P81, and K102 are also with A33, R60, K99, and S109 sites of CRABP2 mutation reported in the COSMIC[53] database (all except K102 highlighted in green in Figure 2B). K102 (yellow) is a sumoylation site and is required for estrogen receptor (ER)

Please cite this article in press as: Pastok et al., Structural requirements for the specific binding of CRABP2 to cyclin D3, Structure (2024), https://doi.org/10.1016/j.str.2024.09.020

Table 1. CRABP2 binding to CDK4-cyclin D3 and CDK6-cyclin D3

CRABP2 Mutant[a]	CRABP2 mutant alternative numbering[b]	Mutant selection rationale	K_d CDK4-cyclin D3 [nM][c]	K_d CDK6-cyclin D3 [nM][c]
Wild type CRABP2	N/A	N/A	118 ± 49	113 ± 60
K21A K21D	K20A K20D	NLS[d]	80.5 ± 11 ND[e]	101 ± 10 ND
R30A/K31A or R30D/K31D	R29A/K30A or R29D/K30D	NLS[d]	ND	ND
A33D	–	COSMIC[f]	23.7 ± 0.4	28.5 ± 0.9
R60D	–	COSMIC	28.8 ± 3.3	31.2 ± 1.9
Q75K Q75E	–	Residue difference with CRABP1, COSMIC	31.2 ± 6.4 40.5 ± 0.7	34.6 ± 13.3 50.7 ± 7.1
P81K	P80	Residue difference with CRABP1	42.8 ± 2.1	38.4 ± 2.0
K99A K99D	K100	Residue difference with CRABP1	38.9 ± 1.5 40.9 ± 0.4	50.9 ± 8.2 55.2 ± 5.1
K102A K102D	K103	Residue difference with CRABP1; Reported SUMOylation site Requirement for ER release	43.5 ± 2.0 59.8 ± 3.3	56.2 ± 5.3 128 ± 10
K107A	K106A	surface	29.5 ± 1.6	36.9
S109L	–	COSMIC	19.1 ± 0.5	24.1 ± 0.4
R112D	R111D	RA[g] binding	42.0 ± 10.5	64.1
R112A/E113A/L114A	R111A/E112A/L113A	RA binding	111 ± 6	146 ± 30
Q75K/K102A	–	RAR[h,i] binding	47.9 ± 1.5	41.4 ± 1.5
P81K/K102D	–	RAR binding	83.3 ± 3.0	84.1 ± 4.3
Q75K/P81K/K102A	–	RAR binding	46.0 ± 1.9	19.8 ± 2.1

[a]CRABP2 numbering according to UniProt entry P29373.
[b]CRABP2 numbering as reported in a literature subset.
[c]K_d was estimated based on at least 2 different experiments performed on different days. Errors represent the SD from the mean. If no standard deviation is provided, then the experiment was performed once.
[d]NLS. Non-classical nuclear localization signal.
[e]ND. No binding detected.
[f]COSMIC. Reported in the Compendium of Somatic Mutations in Cancer database.
[g]RA. Retinoic acid.
[h]CRABP2 mutant Q75E/P81K/K102E does not bind to RAR.[34]
[i]RAR. Retinoic acid receptor.

release.[54] We also mutated K21, R30, and K31 (blue) that form the non-canonical NLS required for CRABP2 interaction with importin α[30] and K107 (pink) implicated in the CRABP2-HuR interaction.[55] Finally, we tested CRABP2 mutants that block RA binding; R112 which lies at the base of the RA binding site (R112D) (red), and the triple mutant R112A/E113A/L114A.[5,26]

The binding of each of these mutants to CDK4-cyclin D3 and CDK6-cyclin D3 was again assessed by HTRF (Table 1). Mutation of CRABP2 R112 to an aspartate which lies at the base of the RA binding site, or the triple mutant R112/E113/L114 to AAA did not significantly affect cyclin D3 association (K_ds CRABP2 R112D and the triple mutant vs. CDK4-cyclin D3, 42.0 ± 10.5 nM and 111 ± 6 nM respectively, Figures 2C and 2D) but as predicted markedly reduced RA binding (Figure S2A).[5] Mutations to residues implicated in RAR binding (Q75, P81, and K102), individually or in combination (Figures S2B and S2C), at residues identified in the COSMIC database (A33, R60, and S109) or at the proposed HuR binding site (K107) (Figures 2C and 2D) similarly did not affect binding to cyclin D3 as determined by Kruskal-Wallis tests in comparison to wild type CRABP2 binding and p values >0.2 (Table 1).

In contrast, mutations within the CRABP2 NLS profoundly affected cyclin D3 binding (Figures 2C and 2D). The CRABP2 mutation K21A had little effect ($p > 0.9$) on its interaction with cyclin D3 (K_d = 80.5 ± 11 nM vs. CDK4-cyclin D3 and K_d = 101 ± 10 nM vs. CDK6-cyclin D3) but introducing an aspartate at this position severely reduced binding and binding constants could not be calculated. Mutations to R30 and K31, to either an alanine or aspartate, also resulted in no detectable interaction (Figures 2C and 2D). Mutations in the NLS were also distinguished by their capacity to bind the RA derivative DC271 (Figure S2A). The CRABP2 mutants K21A, K21D, and R30A/K31A bound RA whereas the mutant R30D/K31D did not.

In summary, this mutational study supports a model in which the conformation and the sequence of the helix-loop-helix motif (α1-loop-α2) that caps the RA binding cleft and includes the

Please cite this article in press as: Pastok et al., Structural requirements for the specific binding of CRABP2 to cyclin D3, Structure (2024), https://doi.org/10.1016/j.str.2024.09.020

CellPress
OPEN ACCESS

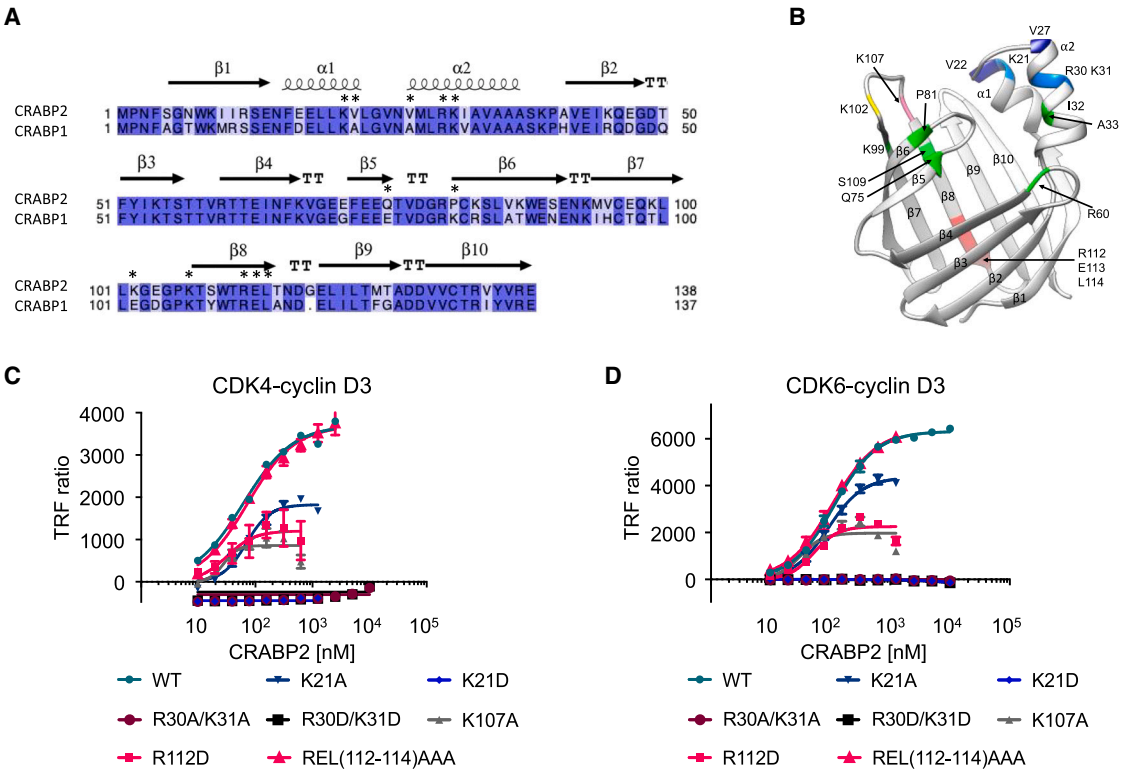

Figure 2. The CRABP2 cyclin D3 binding site overlaps with the nuclear localization sequence

(A) CRABP2 vs. CRABP1 sequence alignment. The locations of secondary structural elements are marked above the sequence, identical residues are highlighted in dark blue, conserved resides in light blue. Residues that are mutated are highlighted with an asterisk.

(B) Locations of CRABP2 residues mutated in this study. Structure PDB 2FS7.[56]

(C and D) Homogeneous time-resolved fluorescence (HTRF) analysis of CRABP2 mutants binding to CDK4-cyclin D3 (C) or CDK6-cyclin D3 (D). The concentrations of CDK4-cyclin D3 and CDK6-cyclin D3 complexes used in the assays were 10 nM. HTRF measurements were carried out in duplicate and repeated on 3 separate days. The error bars indicate SD.

non-canonical NLS distinguishes CRABP2 interactions with its ligand RA and with cyclin D3.

CRABP2 mutants in the NLS promote alternative CRABP2 conformations incompatible with cyclin D3 and retinoic acid binding

To further characterize the CRABP2 structural and sequence requirements for cyclin D3 association, we determined the crystal structures of two CRABP2 variants with mutations in the NLS that together distinguish CRABP2 and RA binding and compared them to the wild-type fold. CRABP2 R30A/K31A binds to RA but does not bind to cyclin D3, whereas CRABP2 R30D/K31D does not bind to either ligand. The structures were determined by molecular replacement using the CRABP2 F15W mutant structure (PDB 2FRS [56]) as a search model at 1.16 Å (CRABP2 R30D/K31D) and 1.33 Å (CRABP2 R30A/K31A), respectively (Table 2).

CRABP2 R30D/K31D adopts a structure in which the α1-loop-α2 "cap" has undergone a significant conformational change (compare Figures 3A and 3B). The second helix (α2) projects down into the hydrophobic cavity, blocking the RA binding site (Figures 3C, S3A, and S3B), and remodeling the motif that mediates cyclin D3 binding. The positioning of the deformed α2 helix forces the displacement of the β sheet regions composed of residues 42–67 (β2, β3, and β4) and residues 72–85 (β5 and partial-β6) (Figure 3C). The CRABP2 hydrophobic cavity, with at its base R112, R133, and Y135 that form the binding site for the carboxylic acid moiety of retinoic acid, is now filled by the aliphatic side-chains of I32, V34, A35, and A36 (compare Figures 3D and 3E, sequence highlighted in green). These residues now lead into an extended loop preceding β2 as α2 is shortened (residues 29–35 vs. 27–37 in the authentic fold). In the authentic structure R30 and K31 are both solvent exposed (Figure 3A). The mutated residues, on opposed sides of the reformed α2 helix, are buried (D31) and exposed to the surface (D30), respectively (Figures 3B and 3C). M28, E74, Q98, and W110 enclose D31, the closest approach being made by the side-chain amide moiety of Q98 (Figure 3F). To allow for this remodeling relative to the wild type protein, the loop between α1 and α2 is lengthened (residues 23–29 vs. 23–27 in the authentic fold).

These two mutated residues, with opposite charges to their wild-type counterparts, effect a drastic remodeling of the cap region of CRABP2, distorting the overall shape of the protein, occluding the ligand binding site and creating a negative electrostatic surface that would otherwise not be present (Figure S3C). This shift in overall protein character explains the lack of binding to both RA derivatives, and to cyclin D3, which rely on the correct formation of the hydrophobic central binding cavity, and cap region respectively.

Please cite this article in press as: Pastok et al., Structural requirements for the specific binding of CRABP2 to cyclin D3, Structure (2024), https://doi.org/10.1016/j.str.2024.09.020

In contrast, the structure of CRABP2 R30A/K31A overlays well with the authentic CRABP2 fold for most of its sequence (Figure S4A). However, the mutations produce a destabilization in the CRABP2 N terminus that usually wraps around the protein and forms part of the helical cap, resulting in a crystallographic dimer in which the N termini of two monomers are exchanged (Figures S4A and S4B). Within the crystal lattice, a dimer of dimers arrangement is evident in which chains A and B form a domain swapped dimer, itself dimerized with chains C and D (Figure S4C). However, in solution, the protein clearly maintains its expected monomeric state (Figure S4D). This mutant binds to RA under standard assay conditions suggesting a model in which these mutations promote the formation of the dimer, but a population in a conformation compatible with RA binding persists. Crystallization conditions have selected a conformation in which the helix is somewhat collapsed relative to the authentic fold. α2, specifically residues A31-A35, partially occlude the upper opening of the CRABP2 binding site, a location usually occupied by the cyclohexyl head group of retinoic acid. With the exception of α2, there is a good agreement with the authentic protein at nearly all other notable residues, particularly R112, R133, and Y135. Residues from the domain swap event (N2-S13) also maintain good agreement with their wild-type counterparts, when aligned using sub-structure alignment methods (RMSD Cα 1.34 Å).

This behavior is reminiscent of various mutants of human cellular retinol binding protein II (hCRBPII), another member of the iLBP family that has been used as a model system for protein engineering and in which alternative dimer[57] and trimer[58] arrangements have been characterized. Extensive domain swapped hCRBPII dimers were first identified by mutations to residues in the hinge loop region,[59] and this study suggests that this behavior is conserved in CRABP2.

CRABP2 open and collapsed conformations

The R30D/K31D mutant of CRABP2 adopts a conformation with a "collapsed" helical lid, preventing RA and cyclin D3 binding. We hypothesized this conformation may have relevance as an alternate native state, and if so, a model of the collapsed conformation, reverted to a wild-type sequence, should be stable under simulation. If the conformation was unfavored by wild-type *apo* CRABP2, we would anticipate instability and conformational change toward the open conformation seen in the CRABP2 crystal structure (Figure 3). A total of 1.2 μs of productive molecular dynamics simulations were carried out on both open and collapsed conformations of CRABP2 and analyzed, with a particular focus on the movement of the helical lid.

Both open and closed conformations reach a stable state after approximately 100 ns simulation ((Figures 4A and 4B); energetic comparisons provided in Figure S5A). Comparison of the helical lid Cα positions between open and collapsed conformations (Figures 4C and 4D) show these arrangements are stable. Clustering of protein conformations was conducted in GROMACS[60] for the equilibrated period (100–400 ns, dt = 0.5 ns, Figure S5A) with a minimum RMSD of 1.5 Å on superposed Cα positions. Cluster sizes ranged from 6 to 23 from 601 frames, with the key differences observed in the fluctuation of the second helix position (residues 30–41). The average fluctuation of each residue across the replicates for both conformations is compared in Figure 4E. The second helix is highly flexible though on average less mobile in the collapsed conformation, held within the barrel through key hydrogen bonds from K31 to E74 (2.8 Å) and Q97 (3.0 Å) (Figure 4F). This hydrogen bonding pattern mimics that observed in the crystal structure of the R30D/K31D mutant (Figure S5B), where D31 forms hydrogen bonds to the same residues supported by rotation of Q97 at similar distances (3.2 Å and 2.9 Å respectively).

Next, we used sub-sampling of the AlphaFold2 multiple sequence alignment[61] for full-length CRABP2 to produce an ensemble of conformations based on the wild-type sequence, hypothesizing that if accessible, the collapsed conformation would be represented within the predicted landscape. Although the size and rigidity of the CRABP2 protein required very shallow sampling (2:8 or 4:8 *maxseq:extraseq*) to reveal conformers beyond the open conformation (Figure S5C), the collapsed conformation represents 1–3% of those generated (RMSD of residues 15–38 < 3 Å to reference structure, Figure S5D).

Previous studies by NMR on *apo* and ATRA-bound *holo* CRABP2[62] demonstrated widespread dynamic movement of *apo* CRABP2 on the micro- to millisecond timescale, with particularly large exchange dynamics for the R30 and K31 residues. Lixa et al. suggested the crystallized open *apo* conformation of CRABP2 represents a dominant conformation within the ensemble, where the conformational fluctuation of CRABP2 is critical for regulation. The stability of our collapsed *apo* conformation under 1.2 μs simulation indicates this could represent a less dominant but distinct conformation within that dynamic *apo* CRABP2 ensemble.

AlphaFold model of the CDK4-cyclin D3-CRABP2 complex

The CRABP2 mutational study identifies residues within the α1-loop-α2 cap as important for cyclin D3 binding. However, given the large-scale changes to the CRABP2 structure observed for those mutants for which structures were determined, it could not be discounted that the effects of mutations on cyclin D3 binding could be indirect. To further support our proposed model of the cyclin D3-CRABP2 interaction, we utilized AlphaFold2-Multimer via Colab[51,63] to generate a model of the cyclin D3-CRABP2 interface (Figures 5A and S6A).

AlphaFold models CDK4-cyclin D3 in the active conformation which aligns closely to the recently reported crystal structure bound to abemaciclib (PDB 7SJ3,[64] cyclin D3:cyclin D3 RMSD 0.7 Å). The predicted CRABP2 structure matches the RA-bound crystal structure, (PDB 1CBQ,[6] RMSD 0.5 Å). This match was expected as AlphaFold uses all existing structures as a template. We then produced a matrix of CDK4/6-D-type cyclin-CRABP2 models from which the predicted aligned error plots (PAE), representing confidence in relative paired amino acid positions were extracted (Figure S6A). CRABP2 interactions with cyclins D1 and D2 bound to CDK4/6 scored highly (low confidence); in contrast low scores (higher confidence) were observed for cyclin D3-containing complexes, corroborating observations that CRABP2 binding is cyclin D3-specific (Figures S6B–S6E). This structure is modeled to form an interface of 821 Å^2 between CRABP2 and cyclin D3. In agreement with the results of our CRABP2 mutation study, the CDK4-cyclin D3-CRABP2 AlphaFold2 model suggests this interaction involves primarily the loop-α2 element of the CRABP2 cap (Figure 5A).

Please cite this article in press as: Pastok et al., Structural requirements for the specific binding of CRABP2 to cyclin D3, Structure (2024), https://doi.org/10.1016/j.str.2024.09.020

Table 2. Data statistics and refinement details

	CRABP2 R30D/K31D	CRABP2 R30A/K31A
Data statistics[a]		
Beamline	I03	I24
Date	21/07/18	08/12/19
Wavelength (Å)	0.9763	0.9686
Resolution (Å)	46.15–1.16 (1.18–1.16)	54.39–1.33 (1.35–1.33)
Space group	I222	$P2_1$
Unit-cell parameters		
a (Å)	45.30	51.17
b (Å)	92.29	106.02
c (Å)	98.76	55.54
α (°)	90.00	90
β (°)	90.00	106.02
γ (°)	90.00	90.00
Unit-cell volume ($Å^3$)	412889	295046
Solvent content (%)	63	48
No. of measured reflections	457763 (9158)	428574 (19438)
No. of independent reflections	71395 (3221)	128510 (6247)
Completeness (%)	99.4 (91.8)	97.1 (94.7)
Redundancy	6.4 (2.8)	3.3 (3.1)
$CC_{1/2}$ (%)	0.999 (0.946)	0.996 (0.411)
<I>/<σ(I)>	19.4 (2.5)	9.7 (1.4)
Refinement statistics		
Rwork (%)	16.24	15.84
Rfree[b] (%)	17.37	19.96
No. of non-H atoms		
No. of protein, atoms	1159	4445
No. of solvent atoms	157	399
No. of ligand atoms	24	4
R.m.s. deviation from ideal values		
Bond angle (°)	1.72	1.86
Bond length (Å)	0.013	0.015
Average B factor (Å2)		
Protein	19	26
Solvent	30	35
Ligand	31	20
Ramachandran plot[c], residues in	–	–
Most favored regions (%)	98.58	98.34
PDB file code	7OXW	7OXX

[a](Values in parenthesis are for the highest resolution shell).
[b]5% of the randomly selected reflections excluded from refinement.
[c]Calculated using MOLPROBITY.[84]

CRABP2 α2 is encased by the C-terminal end of cyclin D3 α1 and two helices from the cyclin D3 C-terminal cyclin box fold (C-CBF, α1′-α5′): α2' (residues 172–191) and the C-terminal end of α5' (highlighted in yellow and orange respectively in Figure 5A). α5' (residues 237–260) is extended by two helical turns in the AlphaFold model as compared to the crystallographically determined cyclin D3 structures (PDBs 3G33 and 7SJ3). At the start of CRABP2 α2, V27 identified previously as contributing to the cyclin D3 interaction, interfaces with cyclin D3 at the end of α1, packing against L65 (4.1 Å) (Figure S7A). Cyclin D3 Y62 also contributes to a solvent exposed hydrophobic face on this helix that CRABP2 occludes in the complex. Moving along the CRABP2 α2 helix, one side packs along its length against cyclin D3 α2′ in an antiparallel fashion: M28 and I32 interface with cyclin D3 L188 (CB:M28 CE 2.9 Å) (which also packs internally within the C-CBF against α5′), and T184 (CA:I32 CG1 3.5 Å), respectively. CRABP2 K31 engages with the C-terminal end of cyclin D3 α1. The side chains of cyclin D3 E69 and E75 in the loop linking cyclin D3 α1-α2 are located 2.4 Å (NZ:OE1) and 3.2 Å (NZ:OE2) away, respectively (Figure S7A). CRABP2 S38 at the end of α2 is modeled close to cyclin D3 L177 (OG:CD1 3.0 Å). CRABP2 α2 also packs across the last two modeled helical turns of cyclin D3 α5' (Figure S7A). L29 and I32 create a hydrophobic face to the helix that complements cyclin D3 residues L251, L255, and A258. CRABP2 L29 and cyclin D3 A258 make the closest contact (CD1:CB 2.5 Å) and I32 and cyclin D3 L251 are modeled 3.5 Å (CD1:CD1) apart.

CRABP2 does not contain a consensus RXL motif found in many cell cycle CDK substrates and regulators (reviewed in Wood and Endicott, 2018).[48] In agreement with the CRABP2 sequence, the model locates CRABP2 at a distance from the cell cycle cyclin RXL recruitment site that in cyclin D3 is centered around W63 within the N-CBF.[48]

To further validate the AlphaFold model, we first truncated cyclin D3 to remove the N- and C-terminal sequences outside the tandem CBFs (ΔC 1–260, ΔN/C 20–260) and designed a set of mutants in which selected sequences were changed to the corresponding residues in cyclin D1, and the conserved cluster of glutamate residues (cyclin D3 E74/E75/E76) was mutated to alanines. These cyclins were co-expressed with CDK4 and binding to CRABP2 was again assessed by HTRF (Figures 5C and S7B; Table 3). The ability of CDK4-cyclin D3 to bind to p27 was not significantly impacted by these cyclin D3 mutations confirming their structural integrity (Figure S7C; Table 3).

In agreement with the model, deletion of either the cyclin D3 C- or N and C-terminal sequences, mutation of W63A (cyclin recruitment site), T194K, 196-AMY-198 to 196-ISN-198 (away from the predicted interface located in the loop linking cyclin D3 α2′-α3′) and 171-PRDRQA-176 at the start of α2′ to 171-GDKNKQ-176 (to resemble the cyclin D1 sequence) did not change the apparent affinity of cyclin D3 for CRABP2 (Figures 5B and S7B). However, as predicted mutating E74, E75, and E76 to alanines abolished the interaction (Figure 5C). This glutamate-rich loop is surface exposed in the CDK4-cyclin D3 apo structure (PDB 3G33) but becomes buried (E76) and binds to the cyclin D3 N-terminal sequence (cyclin D3 R14-E74) on ordering of both this sequence and the CDK4 activation loop in the abemaciclib-bound complex (PDB 7SJ3).

We next tested the ability of a set of cyclin D3 mutants at residues Y62, W63, L65, E69, E75, L251, and L255 to bind to CRABP2 and to p27 using a pull-down assay (Figure 5D,

Please cite this article in press as: Pastok et al., Structural requirements for the specific binding of CRABP2 to cyclin D3, Structure (2024), https://doi.org/10.1016/j.str.2024.09.020

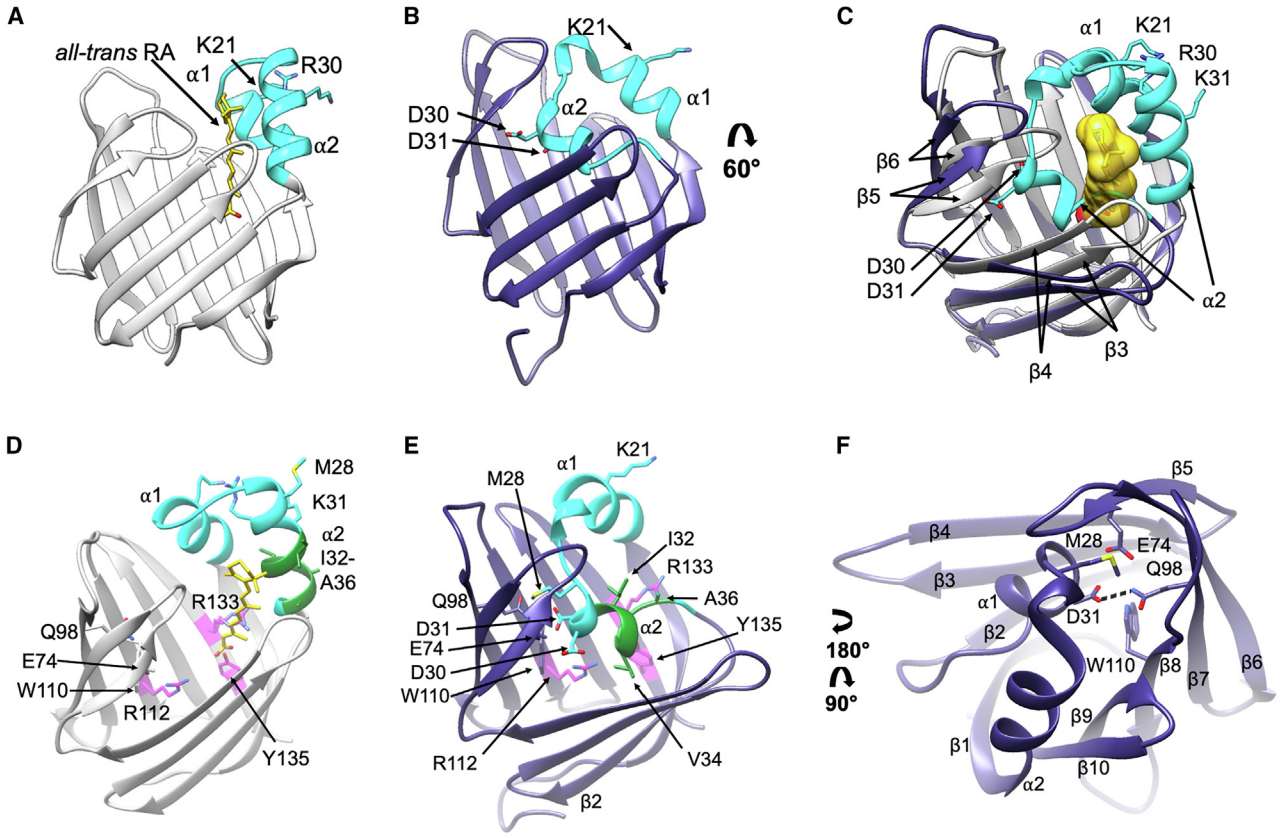

Figure 3. Structure of CRABP2 R30D/K31D reveals an alternative conformation of the retinoic acid binding pocket lid

The CRABP2 R30D/K31D structure (B) is compared with the structure of wild type (WT) CRABP2 bound to ATRA (*all-trans* retinoic acid) (PDB 2FR3), (A). The overlay (C) highlights the relocation and reorganization of the helix-loop-helix lid to occupy the hydrophobic cleft. Changes to the global organization of the CRABP2 fold also accompany mutation of R30 and K31 to aspartate residues. To accommodate changes in the retinoic acid binding pocket, the β sheet composed of β1−β4 and the β5-β6 hairpin are both displaced in the CRABP2 R30D/K31D structure. The side chains of K21, R30, and K31 identify the location of the proposed CRABP2 non-canonical nuclear localization signal.[31]

(D–F) The remodeling of the CRABP2 R30D/R31D retinoic acid binding pocket (E) compared to the WT CRABP2 fold (D).

(F) Close-up of interactions made by D31 within the remodeled retinoic acid binding pocket. The WT CRABP2 and mutant CRABP2 folds are rendered in gray and purple respectively. Side chains of selected amino acids are drawn in ball and stick mode, and ATRA bound to WT CRABP2 is rendered in gold.

uncropped gels (Figures S7D and S7E)). The Y62T/L65A/E69A, Y62T, and L251A/L255K mutants decreased CRABP2 binding with no apparent effect on binding to p27. Of the single site mutants that were tested (Y62T, W63A, E69A, and E75A), cyclin D3 Y62T was the most effective at disrupting CRABP2 binding. Taken together with the HTRF results, our mutant study suggests that cyclin D3 has a protein binding site located in the C-CBF that includes α2′ and the C-terminal end of α5′ and to which residues at the C-terminal end of α1 and in the α1-α2 loop contribute (Figure 5B).

DISCUSSION

Using purified full-length proteins, we have demonstrated that CRABP2 is a cyclin D3-specific binding protein, recognized in the context of cyclin D3 being bound to either CDK4 or CDK6. Through characterization of mutants at known CRABP2-protein interaction sites, we have mapped residues required for cyclin D3 binding to the CRABP2 α1-loop-α2 helical cap. Structure determination of CRABP2 R30D/K31D and CRABP2 R30A/K31A confirms the flexibility of this sequence and reveals alternative CRABP2 folds.

Our molecular dynamics simulations show that the authentic CRABP2 sequence is compatible with the experimentally determined CRABP2 R30D/K31D mutant variant fold we observe. The effect of the mutations can be hypothesized to be a mutation-specific destabilization or to disrupt an authentic equilibrium between alternative native states. They suggest that the collapsed conformation may well be a valid alternative state for wild-type CRABP2, albeit one that requires a specific inducement for conformational change.

Solution studies using NMR have previously revealed that sequences around the entrance to the CRABP2 RA binding pocket undergo conformational exchange between holo- and apo-structures, and in apo-CRABP2 are disordered suggesting structural flexibility in this region that extends to residues in the RA binding pocket.[29] CRABP2 mutations in the RA binding pocket (R111M) and at the start of α1 (F15W) can both promote alternative structures for residues located in apo CRABP2 α2.[28] NMR studies have also suggested CRABP2 dimerization and a

Please cite this article in press as: Pastok et al., Structural requirements for the specific binding of CRABP2 to cyclin D3, Structure (2024), https://doi.org/10.1016/j.str.2024.09.020

CellPress
OPEN ACCESS

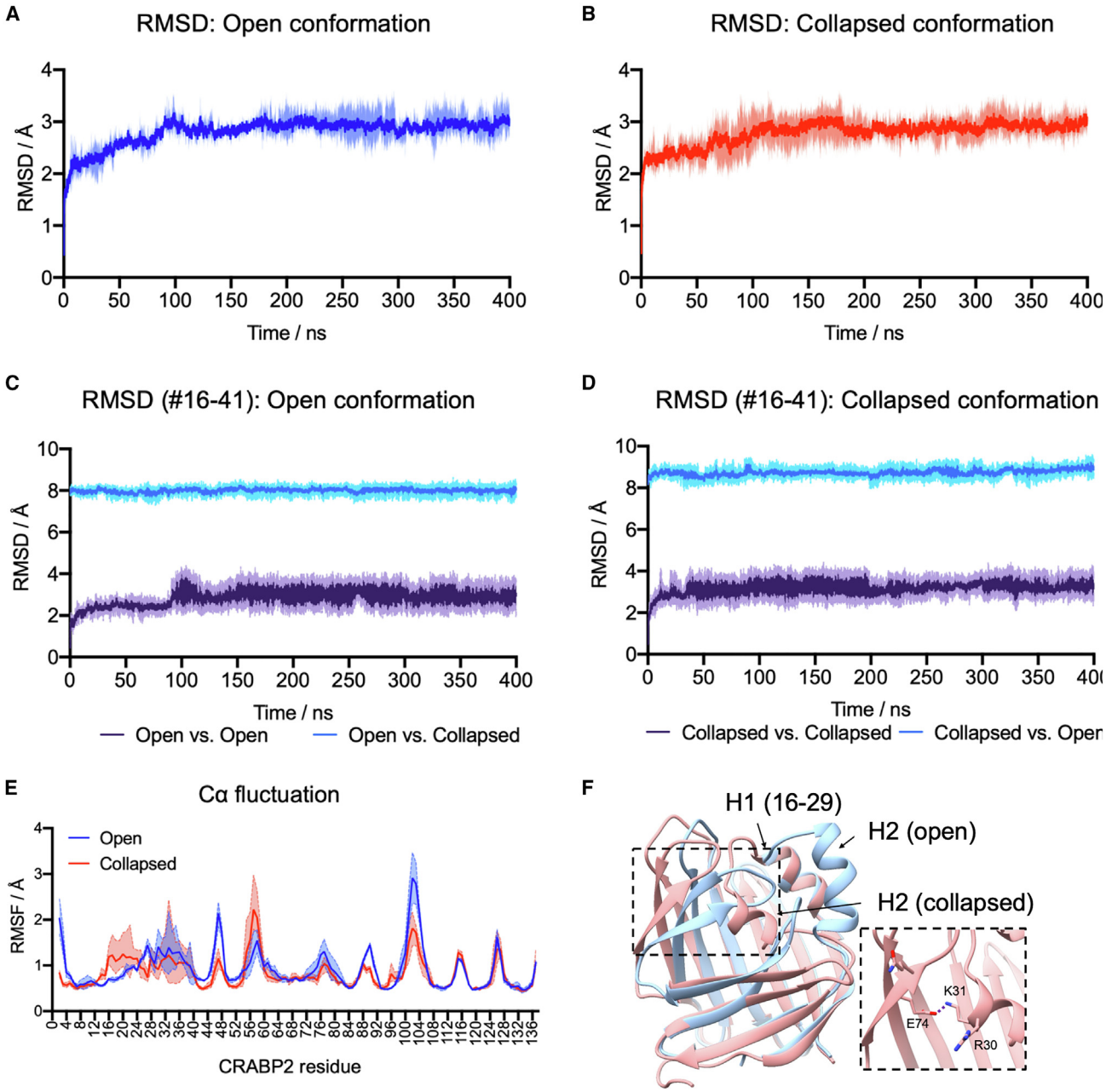

Figure 4. Simulation of the CRABP2 R30/K31 mutant fold

(A–D) Root mean squared deviation plots through simulation time as average of three independent simulations with range depicted as shaded area around mean (strong line), comparing trajectory to energy minimized starting conformation. Panels show (A) RMSD of open conformation simulations; (B) RMSD of collapsed conformation simulations. (C) and (D) show cross-comparisons using only residues 16–41 (the helical lid) to demonstrate the divergence of the conformations and the lack of conformational exchange.

(E) Root mean squared fluctuation of CRABP2 Cα positions for simulation portion 100–400 ns. RMSF shown as average (strong line) of three measurements with area bounded by dashed lines denoting range of three independent simulations.

(F) Representative structures from the open (blue) and collapsed (pink) simulations with H1 and H2 labeled; inset image shows hydrogen bond (2.8 Å) between E74 and K31 and R30 oriented out to solvent.

rigidification of the CRABP2 NLS are promoted upon RA binding, both of which may impact CRABP2 function.[62]

The interaction between CRABP2 and RAR-RXR is mediated by residues at the entrance to the CRABP2 RA binding pocket and the receptor ligand binding domain respectively and has been proposed to promote the transfer of the CRABP2 RA cargo to RARα.[8,36,65] The results presented in this study show that the interaction between CRABP2 and cyclin D3 is also dependent on the conformation of the lid sequence. This functional dependency suggests that cyclin D3 binding may influence the

Please cite this article in press as: Pastok et al., Structural requirements for the specific binding of CRABP2 to cyclin D3, Structure (2024), https://doi.org/10.1016/j.str.2024.09.020

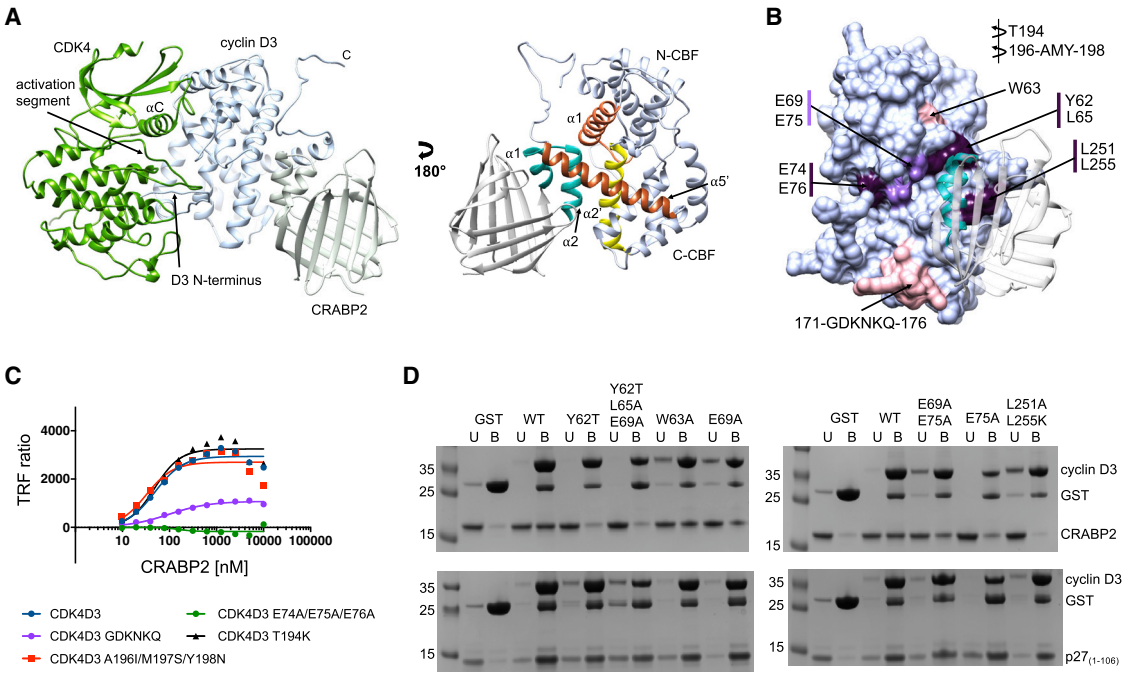

Figure 5. AlphaFold model of the CDK4-cyclin D3-CRABP2 complex

(A) CDK4-cyclin D3-CRABP2 model. The model was generated using AlphaFold2-Multimer via Colab.[51,63] CRABP2, cyclin D3, and CDK4 folds are rendered in gray, pale purple, and green, respectively. In the RHS view, the CRABP2 lid is highlighted in cyan, and cyclin D3 helices α2′ and α5′ in yellow and orange respectively.

(B) Locations of the cyclin D3 mutants that impact CRABP2 binding. Molecular surface of complex with cyclin D3 (in pale purple) with residues that affect binding colored and the CRABP2 structure docked. No impact (W63, GDKNKQ) in pink, low-medium impact in medium purple (E69, E75), high impact (Y62, L65, L251, and L255) in dark purple. C-terminal loop of D3 (260–292) omitted and CRABP2 shown (α1-α2 in cyan) with transparent ribbons for clarity. Mutations T194 and 196-AMY-198, which have no impact on binding, are out of view on opposite face of cyclin D3.

(C) Homogeneous time-resolved fluorescence (HTRF) analysis of CDK6-cyclin D3 wild-type and mutant binding to CRABP2. The concentration of CDK6-cyclin D3 complexes used in the assays were 10 nM. HTRF measurements were carried out in duplicate and repeated on 3 separate days. The error bars indicate SD.

(D) Pull-down analysis to assess CRABP2 binding to CDK6-cyclin D3 wild-type and mutant complexes. Glutathione beads were mixed with baculoviral-infected insect cell lysates expressing CDK6-cyclin D3 complexes, washed extensively and then incubated with excess purified CRABP2. Lower panel, experiment was repeated incubating the washed beads with excess purified p27 (residues 1–106) to confirm the structural integrity of the CDK6-cyclinD3 complexes. Bead bound (B) and unbound (U) fractions were analyzed by SDS-PAGE and visualized by Coomassie staining. Each set of pull-down experiments was carried out using two independently prepared samples of CDK6-cyclin D3 and repeated three times. The samples of CRABP2 and p27 were each from the same purification, but different stock aliquots.

structure or accessibility of this flexible region either by direct binding to the sequence or through allostery. By this mechanism cyclin D3 binding to CRABP2 may impact transfer of RA from CRABP2 to the RA receptor. We hypothesize that this role would be in addition to and may complement cyclin D3's previously proposed roles[36] in either enhancing CRABP2 recruitment on RARα or stabilizing the interaction between CRABP2 and RARα. We note that in our structural model CRABP2 residues proposed to interact with RXR (CRABP2 Q75, P81, and K102) remain solvent accessible suggesting that CRABP2 association with RXR may be compatible with cyclin D3 binding to CRABP2. Interaction of CRABP2 with the nuclear RA receptor does not require CRABP2 to be bound to RA suggesting a structure in which CRABP2 may help maintain nuclear receptor-RA association.[65] Cyclin D3 may remain bound to CRABP2, but its continued interaction with RARα would require RA as reported.[36]

D-type cyclins also regulate other nuclear hormone receptors independently of CDK4/6 by recruitment of co-factors to DNA-bound nuclear hormone receptor complexes.[47] For example, cyclins D1 and D3 inhibit androgen receptor activity,[66] whereas cyclin D1 has been reported as an estrogen receptor activator[67,68] and as a thyroid hormone receptor inhibitor,[69] respectively. In contrast to the RA receptor, these nuclear hormone receptors bind their ligands in the cytoplasm and transport them directly into the nucleus. Cyclin D binding to these hormone receptors is ligand independent and direct, the functional outcome dependent on the identity of cyclin D-recruited cofactors. We note that cyclin D3 L251 is structurally equivalent to cyclin D1 L255 within the LLXXXL sequence (residues 254–259) that interacts with the estrogen receptor LXXLL coactivator recognition motif.[70]

The modeled association of CRABP2 with cyclin D3 leaves the well characterized cyclin RXL motif recruitment site accessible for further protein association. The structures of cyclins A, B, and T illustrate the conservation of a helical binding region within the cyclin C-CBF (Figure S8). In the cyclin A and B structures, this site is occupied by an additional C-terminal helix that follows the C-CBF (residues 408–413 and 398–403, respectively), whereas in the cyclin T-AFF4-Tat complex, helical elements of both

Please cite this article in press as: Pastok et al., Structural requirements for the specific binding of CRABP2 to cyclin D3, Structure (2024), https://doi.org/10.1016/j.str.2024.09.020

Table 3. CDK4-cyclin D3 binding to CRABP2

Cyclin D3 Mutant[a]	Mutant selection rationale	K_d CRABP2 [nM] (HTRF)[b]	K_d p27KIP1 [nM] (HTRF)[b]
Cyclin D3 (1–260)	C-terminal truncation	48 ± 3	23 ± 2
Cyclin D3 (20–260)	N and C-terminal truncation	66 ± 6	-[c]
W63A	RXL recruitment site[d]	146 ± 6	–
T194K	-ve control	48 ± 7	99 ± 87
195-AMY-197 to 195-ISN-197	-ve control	32 ± 6	25 ± 5
171-PRDRQA-176 to 171-GDKNKQ-176	Start α2′ helix	97 ± 10	126 ± 22
E74A/E75A/E76A	E75 at cyclin D3-CRABP2 interface, charged surface patch	ND[e]	33 ± 5

[a]Values for the interactions of wild-type CDK4-cyclin D3 and CDK6-cyclin D3 with CRABP2 are 118 ± 49 and 113 ± 60 nM respectively and are included in Table 1.
[b]K_d was estimated based on at least 2 different experiments performed on different days. Errors represent the SD from the mean.
[c]-, not determined.
[d]Value determined for the interaction between CDK6-cyclin D3 W63A and CRABP2.
[e]ND, not detectable.

AFF4 and Tat bind. Conservation of this site across cyclins suggests that the proposed helical docking site on the cyclin D C-CBF might be more widely employed to mediate cyclin D interactions with other binding proteins. Though the AlphaFold Multimer model has guided the identification of cyclin D3 mutants that locate residues required for CRABP2 binding to the cyclin D3 CBF, identification of the precise location of the CRABP2 binding site on cyclin D3 will require structure determination of the CDK4/6-cyclin D3-CRABP2 ternary complex.

Taken together, our results suggest that both cyclin D3 CBFs encode protein interaction sites. We hypothesize that the C-CBF protein binding site might also be present in cyclins D1 and D2 and as precedented by the functional properties of the N-CBF recruitment site might offer opportunities to modulate cyclin D-protein interactions. Mutually exclusive protein binding to both cyclin binding sites would permit further opportunities to integrate and execute signaling pathways.

RESOURCE AVAILABILITY

Lead contact

Further information and requests for resources and reagents should be directed to and will be fulfilled by the lead contact Jane Endicott (jane.endicott@ncl.ac.uk).

Materials availability

Plasmids for the expression of CRABP1 and CRABP2 (wild type and mutant) are available from the lead contact. Transfer vectors for the expression of CDK4/CDK6 and -cyclin D complexes are available from the lead contact upon completion of an appropriate MTA.

Data and code availability

- All crystallographic data have been deposited at the Protein Data Bank (PDB) https://www.rcsb.org/ and are publicly available. Accession numbers are listed in the key resources table. PDB accession codes for structures used within, but not derived from, this study: PDB: 2FRS (F15W mutant of apo-CRABP2 at 1.51 Å resolution), PDB: 2FS7 (apo-CRABP2 at 1.55 Å resolution), PDB: 1CBQ (RA-bound CRABP2 at 2.20 Å resolution), PDB: 2CBS (RO-13 6307 bound CRABP2 at 2.1 Å resolution), PDB: 2W9F (CDK4-cyclin D1 at 2.85 Å resolution), PDB: 3G33 (CDK4-cyclin D3 at 3.00 Å resolution), PDB: 7SJ3 (CDK4-cyclin D3-abemaciclib at 2.51 Å resolution). Biophysical assay (retinoid binding, HTRF, and DSF) and molecular dynamics and AlphaFold Multimer modeling data reported in this paper will be shared by the lead contact upon request.
- This paper does not report original code.
- Any additional information required to reanalyze the data reported in this paper is available from the lead contact upon request.

ACKNOWLEDGMENTS

We thank staff at the Diamond DLS synchrotron (Oxfordshire, UK) for providing excellent facilities at beamlines I03 and I24 (proposal MX18598). We also thank Corinne Wills from the NMR facility, Newcastle University Chemistry Department for NMR data collection and help with data analysis, Claire Jennings for mass spectrometry support and Richard Heath for construction of the BirA expression plasmid. This research was supported by the MRC (grant references MR/N009738/1, M.W.P., J.A.E., and M.E.M.N., and MR/V029142/1, S.T., J.A.E., and M.E.M.N.), an MRC CASE award to C.W.E.T. (MR/N0186481/1) and an EPSRC CDT MoSMed studentship (EP/S022791/1) to A.Bu.). NT position within the Newcastle Drug Discovery Group is supported by Astex Pharmaceuticals. For the purpose of open access, the authors have applied a Creative Commons Attribution (CC BY) licence to any Author Accepted Manuscript version arising from this submission.

AUTHOR CONTRIBUTIONS

M.W.P.: construct design, protein production, biophysical methods (SEC, SPR, ITC, HTRF) and X-ray crystallography (crystallization and structural solution), and to whom correspondence on structural and biophysical aspects of this work should be addressed; A.Bu.: protein production and biophysical methods (HTRF); S.T.: construct design, protein production, and biophysical methods (HTRF and pulldowns); A.Ba.; data collection, Diamond Light Source; C.W.E.T.: protein production, biochemical assays, and X-ray crystallography (data collection and structural solution); N.J.T.: MD simulations and AlphaFold modeling and to whom correspondence on computational aspects of this work should be addressed; E. P., M.E.M.N., and J.A.E.: conceptualization, resources, supervision, and funding acquisition; all authors contributed to the design of the project, analyzed the data, and wrote the paper.

DECLARATION OF INTERESTS

Some work in the authors' laboratory is supported by a research grant from Astex Pharmaceuticals.

STAR★METHODS

Detailed methods are provided in the online version of this paper and include the following:

- KEY RESOURCES TABLE
- EXPERIMENTAL MODEL AND STUDY PARTICIPANT DETAILS
  - *In vitro* studies
- METHOD DETAILS
  - Protein expression
  - Protein purification
  - Protein structure determination
  - Retinoid binding assay
  - CRABP1 and CRABP2 biotinylation
  - Homogenous time-resolved fluorescence (HTRF)
  - Analytical size exclusion chromatography
  - Protein complex detection by pulldown
  - Structural analysis of iLBP family members
  - Molecular dynamics simulations
  - AlphaFold Multimer modelling
  - AlphaFold Multimer sub-sampling
- QUANTIFICATION AND STATISTICAL ANALYSIS
  - Retinoid binding assay
  - Homogenous time-resolved fluorescence
  - Analytical size exclusion chromatography
  - Protein complex determination by pulldown
  - Molecular dynamics simulations
  - AlphaFold Multimer modelling
  - AlphaFold Multimer sub-sampling
  - X-ray data collection and analysis

SUPPLEMENTAL INFORMATION

Supplemental information can be found online at https://doi.org/10.1016/j.str.2024.09.020.

Received: December 15, 2021
Revised: July 31, 2024
Accepted: September 20, 2024
Published: October 16, 2024; corrected online: October 22, 2024

REFERENCES

1. Napoli, J.L. (2017). Cellular retinoid binding-proteins, CRBP, CRABP, FABP5: Effects on retinoid metabolism, function and related diseases. Pharmacol. Ther. *173*, 19–33. https://doi.org/10.1016/j.pharmthera.2017.01.004.
2. Banaszak, L., Winter, N., Xu, Z., Bernlohr, D.A., Cowan, S., and Jones, T.A. (1994). Lipid-binding proteins: a family of fatty acid and retinoid transport proteins. Adv. Protein Chem. *45*, 89–151.
3. Veerkamp, J.H., Peeters, R.A., and Maatman, R.G. (1991). Structural and functional features of different types of cytoplasmic fatty acid-binding proteins. Biochim. Biophys. Acta *1081*, 1–24. https://doi.org/10.1016/0005-2760(91)90244-C.
4. Veerkamp, J.H., and Maatman, R.G. (1995). Cytoplasmic fatty acid-binding proteins: Their structure and genes. Prog. Lipid Res. *34*, 17–52. https://doi.org/10.1016/0163-7827(94)00005-7.
5. Chen, X., Tordova, M., Gilliland, G.L., Wang, L., Li, Y., Yan, H., and Ji, X. (1998). Crystal structure of apo-cellular retinoic acid-binding protein type II (R111M) suggests a mechanism of ligand entry. J. Mol. Biol. *278*, 641–653. https://doi.org/10.1006/jmbi.1998.1734.
6. Kleywegt, G.J., Bergfors, T., Senn, H., Le Motte, P., Gsell, B., Shudo, K., and Jones, T.A. (1994). Crystal structures of cellular retinoic acid binding proteins I and II in complex with all-trans-retinoic acid and a synthetic retinoid. Structure *2*, 1241–1258. https://doi.org/10.1016/S0969-2126(94)00125-1.
7. Tomlinson, C.W.E., Cornish, K.A.S., Whiting, A., and Pohl, E. (2021). Structure–functional relationship of cellular retinoic acid-binding proteins I and II interacting with natural and synthetic ligands. Acta Crystallogr. D Struct. Biol. *77*, 164–175. https://doi.org/10.1107/S2059798320015247.
8. Dong, D., Ruuska, S.E., Levinthal, D.J., and Noy, N. (1999). Distinct roles for cellular retinoic acid-binding proteins I and II in regulating signaling by retinoic acid. J. Biol. Chem. *274*, 23695–23698. https://doi.org/10.1074/jbc.274.34.23695.
9. Budhu, A.S., and Noy, N. (2002). Direct Channeling of Retinoic Acid between Cellular Retinoic Acid-Binding Protein II and Retinoic Acid Receptor Sensitizes Mammary Carcinoma Cells to Retinoic Acid-Induced Growth Arrest. Mol. Cell Biol. *22*, 2632–2641. https://doi.org/10.1128/mcb.22.8.2632-2641.2002.
10. Delva, L., Bastie, J.-N., Rochette-Egly, C., Kraïba, R., Balitrand, N., Despouy, G., Chambon, P., and Chomienne, C. (1999). Physical and Functional Interactions between Cellular Retinoic Acid Binding Protein II and the Retinoic Acid-Dependent Nuclear Complex. Mol. Cell Biol. *19*, 7158–7167. https://doi.org/10.1128/mcb.19.10.7158.
11. Donato, L.J., Suh, J.H., and Noy, N. (2007). Suppression of mammary carcinoma cell growth by retinoic acid: The cell cycle control gene Btg2 is a direct target for retinoic acid receptor signaling. Cancer Res. *67*, 609–615. https://doi.org/10.1158/0008-5472.CAN-06-0989.
12. Manor, D., Shmidt, E.N., Budhu, A., Flesken-Nikitin, A., Zgola, M., Page, R., Nikitin, A.Y., and Noy, N. (2003). Mammary carcinoma suppression by cellular retinoic acid binding protein-II. Cancer Res. *63*, 4426–4433.
13. Pohl, E., and Tomlinson, C.W.E. (2020). Classical pathways of gene regulation by retinoids. Methods Enzymol. *637*, 151–173. https://doi.org/10.1016/BS.MIE.2020.03.008.
14. Vreeland, A.C., Yu, S., Levi, L., de Barros Rossetto, D., and Noy, N. (2014). Transcript Stabilization by the RNA-Binding Protein HuR Is Regulated by Cellular Retinoic Acid-Binding Protein 2. Mol. Cell Biol. *34*, 2135–2146. https://doi.org/10.1128/mcb.00281-14.
15. Liu, R.Z., Li, S., Garcia, E., Glubrecht, D.D., Poon, H.Y., Easaw, J.C., and Godbout, R. (2016). Association between cytoplasmic CRABP2, altered retinoic acid signaling, and poor prognosis in glioblastoma. Glia *64*, 963–976. https://doi.org/10.1002/glia.22976.
16. Fischer-Huchzermeyer, S., Dombrowski, A., Hagel, C., Mautner, V.F., Schittenhelm, J., and Harder, A. (2017). The Cellular Retinoic Acid Binding Protein 2 Promotes Survival of Malignant Peripheral Nerve Sheath Tumor Cells. Am. J. Pathol. *187*, 1623–1632. https://doi.org/10.1016/j.ajpath.2017.02.021.
17. Yang, Q., Wang, R., Xiao, W., Sun, F., Yuan, H., and Pan, Q. (2016). Cellular retinoic acid binding protein 2 is strikingly downregulated in human esophageal squamous cell carcinoma and functions as a tumor suppressor. PLoS One *11*, e0148381. https://doi.org/10.1371/journal.pone.0148381.
18. Feng, X., Zhang, M., Wang, B., Zhou, C., Mu, Y., Li, J., Liu, X., Wang, Y., Song, Z., and Liu, P. (2019). CRABP2 regulates invasion and metastasis of breast cancer through hippo pathway dependent on ER status. J. Exp. Clin. Cancer Res. *38*, 361. https://doi.org/10.1186/s13046-019-1345-2.
19. Xiu, Y., Dong, Q., Li, Q., Li, F., Borcherding, N., Zhang, W., Boyce, B., Xue, H.H., and Zhao, C. (2018). Stabilization of NF-κB-Inducing Kinase Suppresses MLL-AF9-Induced Acute Myeloid Leukemia. Cell Rep. *22*, 350–358. https://doi.org/10.1016/j.celrep.2017.12.055.
20. Ross, A.C., and Zolfaghari, R. (2011). Cytochrome P450s in the regulation of cellular retinoic acid metabolism. Annu. Rev. Nutr. *31*, 65–87.
21. Persaud, S.D., Lin, Y.W., Wu, C.Y., Kagechika, H., and Wei, L.N. (2013). Cellular retinoic acid binding protein I mediates rapid non-canonical activation of ERK1/2 by all-trans retinoic acid. Cell. Signal. *25*, 19–25. https://doi.org/10.1016/j.cellsig.2012.09.002.
22. Park, S.W., Nhieu, J., Persaud, S.D., Miller, M.C., Xia, Y., Lin, Y.W., Lin, Y.L., Kagechika, H., Mayo, K.H., and Wei, L.N. (2019). A new regulatory mechanism for Raf kinase activation, retinoic acid-bound Crabp1. Sci. Rep. *9*, 10929. https://doi.org/10.1038/s41598-019-47354-7.

23. Park, S.W., Persaud, S.D., Ogokeh, S., Meyers, T.A., Townsend, D., and Wei, L.N. (2018). CRABP1 protects the heart from isoproterenol-induced acute and chronic remodeling. J. Endocrinol. *236*, 151–165. https://doi.org/10.1530/JOE-17-0613.

24. D'Ambrosio, D.N., Clugston, R.D., and Blaner, W.S. (2011). Vitamin A metabolism: An update. Nutrients *3*, 63–103. https://doi.org/10.3390/nu3010063.

25. Al Tanoury, Z., Piskunov, A., and Rochette-Egly, C. (2013). Vitamin a and retinoid signaling: Genomic and nongenomic effects. J. Lipid Res. *54*, 1761–1775. https://doi.org/10.1194/jlr.R030833.

26. Kleywegt, G.J., Bergfors, T., Senn, H., Le Motte, P., Gsell, B., Shudo, K., and Jones, T.A. (1994). Crystal structures of cellular retinoic acid binding proteins I and II in complex with all trans retinoic acid and a synthetic retinoid. Structure *2*, 1241–1258.

27. Vaezeslami, S., Jia, X., Vasileiou, C., Borhan, B., and Geiger, J.H. (2008). Structural analysis of site-directed mutants of cellular retinoic acid-binding protein II addresses the relationship between structural integrity and ligand binding. Acta Crystallogr. D Biol. Crystallogr. *64*, 1228–1239. https://doi.org/10.1107/S0907444908032216.

28. Vaezeslami, S., Mathes, E., Vasileiou, C., Borhan, B., and Geiger, J.H. (2006). The Structure of Apo-wild-type Cellular Retinoic Acid Binding Protein II at 1.4 Å and its Relationship to Ligand Binding and Nuclear Translocation. J. Mol. Biol. *363*, 687–701. https://doi.org/10.1016/j.jmb.2006.08.059.

29. Wang, L., Li, Y., Abildgaard, F., Markley, J.L., and Yan, H. (1998). NMR solution structure of type II human cellular retinoic acid binding protein: Implications for ligand binding. Biochemistry *37*, 12727–12736. https://doi.org/10.1021/bi9808924.

30. Sessler, R.J., and Noy, N. (2005). A ligand-activated nuclear localization signal in cellular retinoic acid binding protein-II. Mol. Cell *18*, 343–353. https://doi.org/10.1016/j.molcel.2005.03.026.

31. Marfori, M., Mynott, A., Ellis, J.J., Mehdi, A.M., Saunders, N.F.W., Curmi, P.M., Forwood, J.K., Bodén, M., and Kobe, B. (2011). Molecular basis for specificity of nuclear import and prediction of nuclear localization. Biochim. Biophys. Acta *1813*, 1562–1577. https://doi.org/10.1016/j.bbamcr.2010.10.013.

32. Ayers, S.D., Nedrow, K.L., Gillilan, R.E., and Noy, N. (2007). Continuous nucleocytoplasmic shuttling underlies transcriptional activation of PPARγ by FABP4. Biochemistry *46*, 6744–6752. https://doi.org/10.1021/bi700047a.

33. Armstrong, E.H., Goswami, D., Griffin, P.R., Noy, N., and Ortlund, E.A. (2014). Structural basis for ligand regulation of the fatty acidbinding protein 5, peroxisome proliferator-activated receptor β/δ (FABP5-PPARβ/δ) signaling pathway. J. Biol. Chem. *289*, 14941–14954. https://doi.org/10.1074/jbc.M113.514646.

34. Budhu, A., Gillilan, R., and Noy, N. (2001). Localization of the RAR interaction domain of cellular retinoic acid binding protein-II. J. Mol. Biol. *305*, 939–949. https://doi.org/10.1006/jmbi.2000.4340.

35. Nagpal, I., and Wei, L.N. (2019). All-trans retinoic acid as a versatile cytosolic signal modulator mediated by $CRABP_1$. Int. J. Mol. Sci. *20*, 3610. https://doi.org/10.3390/ijms20153610.

36. Despouy, G., Bastie, J.N., Deshaies, S., Balitrand, N., Mazharian, A., Rochette-Egly, C., Chomienne, C., and Delva, L. (2003). Cyclin D3 is a cofactor of retinoic acid receptors, modulating their activity in the presence of cellular retinoic acid-binding protein II. J. Biol. Chem. *278*, 6355–6362. https://doi.org/10.1074/jbc.M210697200.

37. Morgan, D.O. (2007). In The Cell Cycle: Principles of Control, E. Lawrence, ed. (Oxford University Press).

38. Tatum, N.J., and Endicott, J.A. (2020). Chatterboxes: the structural and functional diversity of cyclins. Semin. Cell Dev. Biol. *107*, 4–20. https://doi.org/10.1016/j.semcdb.2020.04.021.

39. Rubin, S.M., Sage, J., and Skotheim, J.M. (2020). Integrating Old and New Paradigms of G1/S Control. Mol. Cell *80*, 183–192. https://doi.org/10.1016/j.molcel.2020.08.020.

40. Nebenfuehr, S., Kollmann, K., and Sexl, V. (2020). The role of CDK6 in cancer. Int. J. Cancer *147*, 2988–2995. https://doi.org/10.1002/ijc.33054.

41. Lee, Y., Dominy, J.E., Choi, Y.J., Jurczak, M., Tolliday, N., Camporez, J.P., Chim, H., Lim, J.H., Ruan, H.B., Yang, X., et al. (2014). Cyclin D1-Cdk4 controls glucose metabolism independently of cell cycle progression. Nature *510*, 547–551. https://doi.org/10.1038/nature13267.

42. Jia, W., Zhao, X., Zhao, L., Yan, H., Li, J., Yang, H., Huang, G., and Liu, J. (2018). Non-canonical roles of PFKFB3 in regulation of cell cycle through binding to CDK4. Oncogene *37*, 1685–1698. https://doi.org/10.1038/s41388-017-0072-4.

43. Hou, X., Zhang, Y., Li, W., Hu, A.J., Luo, C., Zhou, W., Hu, J.K., Daniele, S.G., Wang, J., Sheng, J., et al. (2018). CDK6 inhibits white to beige fat transition by suppressing RUNX1. Nat. Commun. *9*, 1023. https://doi.org/10.1038/s41467-018-03451-1.

44. Pauklin, S., Madrigal, P., Bertero, A., and Vallier, L. (2016). Initiation of stem cell differentiation involves cell cycle-dependent regulation of developmental genes by Cyclin D. Genes Dev. *30*, 421–433. https://doi.org/10.1101/gad.271452.115.

45. Liu, L., Michowski, W., Inuzuka, H., Shimizu, K., Nihira, N.T., Chick, J.M., Li, N., Geng, Y., Meng, A.Y., Ordureau, A., et al. (2017). G1 cyclins link proliferation, pluripotency and differentiation of embryonic stem cells. Nat. Cell Biol. *19*, 177–188. https://doi.org/10.1038/ncb3474.

46. Tigan, A.S., Bellutti, F., Kollmann, K., Tebb, G., and Sexl, V. (2016). CDK6-a review of the past and a glimpse into the future: From cell-cycle control to transcriptional regulation. Oncogene *35*, 3083–3091. https://doi.org/10.1038/onc.2015.407.

47. Hydbring, P., Malumbres, M., and Sicinski, P. (2016). Non-canonical functions of cell cycle cyclins and cyclin-dependent kinases. Nat. Rev. Mol. Cell Biol. *17*, 280–292. https://doi.org/10.1038/NRM.2016.27.

48. Wood, D.J., and Endicott, J.A. (2018). Structural insights into the functional diversity of the CDK–cyclin family. Open Biol. *8*, 180112. https://doi.org/10.1098/rsob.180112.

49. Satyanarayana, A., and Kaldis, P. (2009). Mammalian cell-cycle regulation: several Cdks, numerous cyclins and diverse compensatory mechanisms. Oncogene *28*, 2925–2939. https://doi.org/10.1038/onc.2009.170.

50. Martínez-Alonso, D., and Malumbres, M. (2020). Mammalian cell cycle cyclins. Semin. Cell Dev. Biol. *107*, 28–35. https://doi.org/10.1016/j.semcdb.2020.03.009.

51. Mirdita, M., Schütze, K., Moriwaki, Y., Heo, L., Ovchinnikov, S., and Steinegger, M. (2022). ColabFold: making protein folding accessible to all. Nat. Methods *19*, 679–682. https://doi.org/10.1038/s41592-022-01488-1.

52. Hallett, S.T., Pastok, M.W., Morgan, R.M.L., Wittner, A., Blundell, K.L.I.M., Felletar, I., Wedge, S.R., Prodromou, C., Noble, M.E.M., Pearl, L.H., and Endicott, J.A. (2017). Differential Regulation of G1 CDK Complexes by the Hsp90-Cdc37 Chaperone System. Cell Rep. *21*, 1386–1398. https://doi.org/10.1016/j.celrep.2017.10.042.

53. Sondka, Z., Dhir, N.B., Carvalho-Silva, D., Jupe, S., Madhumita, McLaren, K., Starkey, M., Ward, S., Wilding, J., Ahmed, M., et al. (2024). COSMIC: a curated database of somatic variants and clinical data for cancer. Nucleic Acids Res. *52*, D1210–D1217. https://doi.org/10.1093/nar/gkad986.

54. Majumdar, A., Petrescu, A.D., Xiong, Y., and Noy, N. (2011). Nuclear translocation of cellular retinoic acid-binding protein II is regulated by retinoic acid-controlled SUMOylation. J. Biol. Chem. *286*, 42749–42757. https://doi.org/10.1074/jbc.M111.293464.

55. Vreeland, A., Driscoll, D., and Noy, N. (2018). Dissecting the dual activity of cellular retinoic acid binding protein (CRABP2). Faseb. J. *31*, lb148. https://doi.org/10.1096/fasebj.31.1.supplement.lb148.

56. Vaezeslami, S., Mathes, E., Vasileiou, C., Borhan, B., and Geiger, J.H. (2006). The structure of Apo-wild-type cellular retinoic acid binding protein II at 1.4 A and its relationship to ligand binding and nuclear translocation. J. Mol. Biol. *363*, 687–701. https://doi.org/10.1016/J.JMB.2006.08.059.

57. Ghanbarpour, A., Pinger, C., Esmatpour Salmani, R., Assar, Z., Santos, E.M., Nosrati, M., Pawlowski, K., Spence, D., Vasileiou, C., Jin, X., et al.

(2019). Engineering the hCRBPII Domain-Swapped Dimer into a New Class of Protein Switches. J. Am. Chem. Soc. *141*, 17125–17132. https://doi.org/10.1021/jacs.9b04664.

58. Ghanbarpour, A., Santos, E.M., Pinger, C., Assar, Z., Hossaini Nasr, S., Vasileiou, C., Spence, D., Borhan, B., and Geiger, J.H. (2020). Human Cellular Retinol Binding Protein II Forms a Domain-Swapped Trimer Representing a Novel Fold and a New Template for Protein Engineering. Chembiochem *21*, 3192–3196. https://doi.org/10.1002/cbic.202000405.

59. Assar, Z., Nossoni, Z., Wang, W., Santos, E.M., Kramer, K., McCornack, C., Vasileiou, C., Borhan, B., and Geiger, J.H. (2016). Domain-Swapped Dimers of Intracellular Lipid-Binding Proteins: Evidence for Ordered Folding Intermediates. Structure *24*, 1590–1598. https://doi.org/10.1016/j.str.2016.05.022.

60. Abraham, M.J., Murtola, T., Schulz, R., Páll, S., Smith, J.C., Hess, B., and Lindahl, E. (2015). Gromacs: High performance molecular simulations through multi-level parallelism from laptops to supercomputers. SoftwareX *1–2*, 19–25. https://doi.org/10.1016/j.softx.2015.06.001.

61. Monteiro da Silva, G., Cui, J.Y., Dalgarno, D.C., Lisi, G.P., and Rubenstein, B.M. (2024). High-throughput prediction of protein conformational distributions with subsampled AlphaFold2. Nat. Commun. *15*, 2464. https://doi.org/10.1038/s41467-024-46715-9.

62. Lixa, C., Clarkson, M.W., Iqbal, A., Moon, T.M., Almeida, F.C.L., Peti, W., and Pinheiro, A.S. (2019). Retinoic Acid Binding Leads to CRABP2 Rigidification and Dimerization. Biochemistry *58*, 4183–4194. https://doi.org/10.1021/ACS.BIOCHEM.9B00672.

63. Jumper, J., Evans, R., Pritzel, A., Green, T., Figurnov, M., Ronneberger, O., Tunyasuvunakool, K., Bates, R., Žídek, A., Potapenko, A., et al. (2021). Highly accurate protein structure prediction with AlphaFold. Nature *596*, 583–589. https://doi.org/10.1038/s41586-021-03819-2.

64. Gharbi, S.I., Pelletier, L.A., Espada, A., Gutiérrez, J., Sanfeliciano, S.M.G., Rauch, C.T., Ganado, M.P., Baquero, C., Zapatero, E., Zhang, A., et al. (2022). Crystal structure of active CDK4-cyclin D and mechanistic basis for abemaciclib efficacy. NPJ Breast Cancer *8*, 126. https://doi.org/10.1038/S41523-022-00494-Y.

65. Bastie, J.N., Despouy, G., Balitrand, N., Rochette-Egly, C., Chomienne, C., and Delva, L. (2001). The novel co-activator CRABPII binds to RARα and RXRα via two nuclear receptor interacting domains and does not require the AF-2 "core.". FEBS Lett. *507*, 67–73. https://doi.org/10.1016/S0014-5793(01)02938-6.

66. Petre, C.E., Wetherill, Y.B., Danielsen, M., and Knudsen, K.E. (2002). Cyclin D1: mechanism and consequence of androgen receptor co-repressor activity. J. Biol. Chem. *277*, 2207–2215. https://doi.org/10.1074/JBC.M106399200.

67. Neuman, E., Ladha, M.H., Lin, N., Upton, T.M., Miller, S.J., DiRenzo, J., Pestell, R.G., Hinds, P.W., Dowdy, S.F., Brown, M., and Ewen, M.E. (1997). Cyclin D1 stimulation of estrogen receptor transcriptional activity independent of cdk4. Mol. Cell Biol. *17*, 5338–5347. https://doi.org/10.1128/mcb.17.9.5338.

68. Zwijsen, R.M., Wientjens, E., Klompmaker, R., Van der Sman, J., Bernards, R., and Michalides, R.J. (1997). CDK-independent activation of estrogen receptor by cyclin D1. Cell *88*, 405–415. https://doi.org/10.1016/S0092-8674(00)81879-6.

69. Lin, H.M., Zhao, L., and Cheng, S.Y. (2002). Cyclin D1 Is a Ligand-independent Co-repressor for Thyroid Hormone Receptors. J. Biol. Chem. *277*, 28733–28741. https://doi.org/10.1074/JBC.M203380200.

70. Savkur, R.S., and Burris, T.P. (2004). The coactivator LXXLL nuclear receptor recognition motif. J. Pept. Res. *63*, 207–212. https://doi.org/10.1111/J.1399-3011.2004.00126.X.

71. Bieniossek, C., Imasaki, T., Takagi, Y., and Berger, I. (2012). MultiBac: Expanding the research toolbox for multiprotein complexes. Trends Biochem. Sci. *37*, 49–57. https://doi.org/10.1016/j.tibs.2011.10.005.

72. Kabsch, W. (2010). XDS. Acta Crystallogr. D Biol. Crystallogr. *66*, 125–132. https://doi.org/10.1107/S0907444909047337.

73. Winter, G., Waterman, D.G., Parkhurst, J.M., Brewster, A.S., Gildea, R.J., Gerstel, M., Fuentes-Montero, L., Vollmar, M., Michels-Clark, T., Young, I.D., et al. (2018). DIALS: Implementation and evaluation of a new integration package. Acta Crystallogr. D Struct. Biol. *74*, 85–97. https://doi.org/10.1107/S2059798317017235.

74. Evans, P.R. (2011). An introduction to data reduction: space-group determination, scaling and intensity statistics. Acta Crystallogr. D Biol. Crystallogr. *67*, 282–292.

75. Evans, P.R., and Murshudov, G.N. (2013). How good are my data and what is the resolution? Acta Crystallogr. D Biol. Crystallogr. *69*, 1204–1214. https://doi.org/10.1107/S0907444913000061.

76. Winn, M.D., Ballard, C.C., Cowtan, K.D., Dodson, E.J., Emsley, P., Evans, P.R., Keegan, R.M., Krissinel, E.B., Leslie, A.G.W., McCoy, A., et al. (2011). Overview of the CCP4 suite and current developments. Acta Crystallogr. D Biol. Crystallogr. *67*, 235–242.

77. Potterton, L., Agirre, J., Ballard, C., Cowtan, K., Dodson, E., Evans, P.R., Jenkins, H.T., Keegan, R., Krissinel, E., Stevenson, K., et al. (2018). CCP4i2: the new graphical user interface to the CCP4 program suite. Acta Crystallogr. D Struct. Biol. *74*, 68–84.

78. Krissinel, E., Uski, V., Lebedev, A., Winn, M., and Ballard, C. (2018). Distributed computing for macromolecular crystallography. Acta Crystallogr. D Struct. Biol. *74*, 143–151. https://doi.org/10.1107/S2059798317014565.

79. McCoy, A.J., Grosse-Kunstleve, R.W., Adams, P.D., Winn, M.D., Storoni, L.C., and Read, R.J. (2007). Phaser crystallographic software. J. Appl. Crystallogr. *40*, 658–674. https://doi.org/10.1107/S0021889807021206.

80. Vagin, A., and Teplyakov, A. (1997). MOLREP: an automated program for molecular replacement. J. Appl Cryst *30*, 1022–1025.

81. Cowtan, K. (2008). Fitting molecular fragments into electron density. Acta Crystallogr. D Biol. Crystallogr. *64*, 83–89. https://doi.org/10.1107/S0907444907033938.

82. Murshudov, G.N., Skubák, P., Lebedev, A.A., Pannu, N.S., Steiner, R.A., Nicholls, R.A., Winn, M.D., Long, F., and Vagin, A.A. (2011). REFMAC5 for the refinement of macromolecular crystal structures. Acta Crystallogr. D Biol. Crystallogr. *67*, 355–367. https://doi.org/10.1107/S0907444911001314.

83. Emsley, P., Lohkamp, B., Scott, W.G., and Cowtan, K. (2010). Features and development of Coot. Acta Crystallogr. D Biol. Crystallogr. *66*, 486–501. https://doi.org/10.1107/S0907444910007493.

84. Williams, C.J., Headd, J.J., Moriarty, N.W., Prisant, M.G., Videau, L.L., Deis, L.N., Verma, V., Keedy, D.A., Hintze, B.J., Chen, V.B., et al. (2018). MolProbity: More and better reference data for improved all-atom structure validation. Protein Sci. *27*, 293–315. https://doi.org/10.1002/pro.3330.

85. Meng, E.C., Goddard, T.D., Pettersen, E.F., Couch, G.S., Pearson, Z.J., Morris, J.H., and Ferrin, T.E. (2023). UCSF ChimeraX: Tools for structure building and analysis. Protein Sci. *32*, e4792. https://doi.org/10.1002/PRO.4792.

86. Madeira, F., Park, Y.M., Lee, J., Buso, N., Gur, T., Madhusoodanan, N., Basutkar, P., Tivey, A.R.N., Potter, S.C., Finn, R.D., and Lopez, R. (2019). The EMBL-EBI search and sequence analysis tools APIs in 2019. Nucleic Acids Res. *47*, W636–W641. https://doi.org/10.1093/nar/gkz268.

87. Sievers, F., and Higgins, D.G. (2018). Clustal Omega for making accurate alignments of many protein sequences. Protein Sci. *27*, 135–145. https://doi.org/10.1002/pro.3290.

88. Waterhouse, A.M., Procter, J.B., Martin, D.M.A., Clamp, M., and Barton, G.J. (2009). Jalview Version 2 - a multiple sequence alignment editor and analysis workbench. Bioinformatics *25*, 1189–1191.

89. Robert, X., and Gouet, P. (2014). Deciphering key features in protein structures with the new ENDscript server. Nucleic Acids Res. *42*, 320–324. https://doi.org/10.1093/nar/gku316.

90. Pettersen, E.F., Goddard, T.D., Huang, C.C., Couch, G.S., Greenblatt, D.M., Meng, E.C., and Ferrin, T.E. (2004). UCSF Chimera–a visualization

system for exploratory research and analysis. J. Comput. Chem. *25*, 1605–1612. https://doi.org/10.1002/jcc.20084.

91. Hornak, V., Abel, R., Okur, A., Strockbine, B., Roitberg, A., and Simmerling, C. (2006). Comparison of multiple Amber force fields and development of improved protein backbone parameters. Proteins *65*, 712–725. https://doi.org/10.1002/prot.21123.

92. Harris, C.R., Millman, K.J., van der Walt, S.J., Gommers, R., Virtanen, P., Cournapeau, D., Wieser, E., Taylor, J., Berg, S., Smith, N.J., et al. (2020). Array programming with NumPy. Nature *585*, 357–362. https://doi.org/10.1038/s41586-020-2649-2.

93. Michaud-Agrawal, N., Denning, E.J., Woolf, T.B., and Beckstein, O. (2011). MDAnalysis: A toolkit for the analysis of molecular dynamics simulations. J. Comput. Chem. *32*, 2319–2327. https://doi.org/10.1002/JCC.21787.

94. Redfern, C.P., and Wilson, K.E. (1993). Ligand binding properties of human cellular retinoic acid binding protein II expressed in E. coli as a glutathione-S-transferase fusion protein. FEBS Lett. *321*, 163–168. https://doi.org/10.1016/0014-5793(93)80100-9.

Please cite this article in press as: Pastok et al., Structural requirements for the specific binding of CRABP2 to cyclin D3, Structure (2024), https://doi.org/10.1016/j.str.2024.09.020

STAR★METHODS

KEY RESOURCES TABLE

REAGENT or RESOURCE	SOURCE	IDENTIFIER
Antibodies		
Tb-anti-GST antibody	Revvity	Cat# 61GSTTLB; RRID: AB_3662094
Bacterial and virus strains		
E. coli DH5α	Invitrogen	18265-017
E. coli BL21STAR™ (DE3)	ThermoFisher Scientific	C601003
E. coli Rosetta2 (DE3) pLYS-S	Novagen	709564
E. coli DH10EmBacY	Geneva Biotech	Supplied as part of MultiBac™ Expression System Kit
Chemicals, peptides, and recombinant proteins		
Streptavidin-labelled XL665	CisBio	610SAXLB
Critical commercial assays		
MultiBac™ Expression System Kit	Geneva Biotech	N/A
GeneJuice® Transfection reagent	Merck Millipore	70967
Insect-Xpress insect cells medium	Lonza	BELN12-730Q
QuikChangeII Site-Directed Mutagenesis Kit	Agilent	200523
Deposited data		
Crystal structure of CRABP2_R30D/K31D	This paper	PDB entry 7OXW
Crystal structure of CRABP2_R30A/K31A	This paper	PDB entry 7OXX
Experimental models: Cell lines		
Spodoptera frugiperda Sf9 cells	OET	600100
Oligonucleotides		
Primers used in this study please see Table S2 (Eurofins Genomics Ltd)	This paper	N/A
Recombinant DNA		
pACEBac1-GST-CDK4	Hallett et al. [52]	N/A
pACEBac1-GST-CDK6	Hallett et al. [52]	N/A
pIDK-cyclin D1	Hallett et al. [52]	N/A
pIDK-cyclin D3	Hallett et al. [52]	N/A
pIDS-p21	This paper	N/A
Human CRABP1	Tomlinson et al. [7]	N/A
Human CRABP2	Horizon Discovery	MHS6278-202826787
Human CRABP2 K21A or K21D	This paper	N/A
Human CRABP2 R30A/K31A or R30D/K31D	This paper	N/A
Human CRABP2 A33D	This paper	N/A
Human CRABP2 R60D	This paper	N/A
Human CRABP2 Q75K or Q75E	This paper	N/A
Human CRABP2 P81K	This paper	N/A
Human CRABP2 K99A or K99D	This paper	N/A
Human CRABP2 K102A or K102D	This paper	N/A
Human CRABP2 K107A	This paper	N/A
Human CRABP2 S109L	This paper	N/A
Human CRABP2 R112D or R112M	This paper	N/A
Human CRABP2 R112A/E113A/L114A	This paper	N/A
Human CRABP2 Q75K/K102A	This paper	N/A
Human CRABP2 P81K/K102D	This paper	N/A

(*Continued on next page*)

Please cite this article in press as: Pastok et al., Structural requirements for the specific binding of CRABP2 to cyclin D3, Structure (2024), https://doi.org/10.1016/j.str.2024.09.020

Continued

REAGENT or RESOURCE	SOURCE	IDENTIFIER
Human CRABP2 Q75K/P81K/K102A	This paper	N/A
Human cyclin D3 (1-260)	This paper	N/A
Human cyclin D3 (20-260)	This paper	N/A
Human cyclin D3 W63A	This paper	N/A
Human cyclin D3 (T194K)	This paper	N/A
Human cyclin D3 A195I/M196S/Y197N	This paper	N/A
Human cyclin D3 171-PRDRQA-176 to 171-AEENKQ-176	This paper	N/A
Human cyclin D3 E74A/E75A/E76A	This paper	N/A
Human cyclin D3 E69A	This paper	N/A
Human cyclin D3 E75A	This paper	N/A
Human cyclin D3 E69A/E75A	This paper	N/A
Human cyclin D3 Y62T/L65A/E69A	This paper	N/A
Human cyclin D3 L251A/L255K	This paper	N/A
Human cyclin D3 Y62T	This paper	N/A
Human p27 (1-106)	Hallett et al. [52]	N/A
Human p21 (1-87)	This paper	N/A
Software and algorithms		
GraphPad Prism 9	GraphPad	https://www.graphpad.com
MOLREP (CCP4 suite)	Potterton et al. [77]	www.ccp4.ac.uk
CCP4i2 Suite	Potterton et al. [77]	www.ccp4.ac.uk
Chimera	Pettersen et al. [90]	https://www.cgl.ucsf.edu/chimera/
ChimeraX	Meng et al. [85]	https://www.cgl.ucsf.edu/chimerax/
GROMACS 2020.2	Abraham et al. [60]	https://manual.gromacs.org/documentation/2020/index.html
AMBER99SB forcefield	Harris et al. [92]	https://ambermd.org/AmberModels.php
NumPy	Michaud-Agrawal et al. [93]	https://numpy.org/
Coot	Emsley et al. [83]	https://www2.mrc-lmb.cam.ac.uk/personal/pemsley/coot/
AKTA Unicorn 7 Evaluation software	Cytiva	https://www.cytivalifesciences.com/
JalView2	Waterhouse et al. [88]	www.jalview.org
AlphaFold2-Multimer v.1.3	Mirdita et al. [51]	https://colab.research.google.com/github/sokrypton/ColabFold/blob/main/AlphaFold2.ipynb
AlphaFold2 Subsampling	Monteiro da Silva et al. [61]	https://colab.research.google.com/github/GMdSilva/gms_natcomms_1705932980_data/blob/main/AlphaFold2_Traj_v1.ipynb
MDAnalysis v2.7.0	Redfern et al. [94]	https://www.mdanalysis.org/
Other		
ÄKTA pure chromatography system	Cytiva	N/A
PHERAstar FS	BMG Labtech	N/A
PHERAstar FS excitation filter (337 nm)	BMG Lab tech	N/A
PHERAstar FS emission filter (620/665 nm)	BMG Labtech	N/A

EXPERIMENTAL MODEL AND STUDY PARTICIPANT DETAILS

In vitro studies

DNA vectors to express recombinant proteins used in this study were prepared from strain *E. coli* DH5α (for *E. coli*-based expression systems) or *E. coli* DH10EmBacY for generation of recombinant transfer vectors for protein expression in insect cells. Proteins were expressed from recombinant *E. coli* BL21STAR™ (DE3), or Rosetta2 (DE3) pLYS-S or baculoviral infected *Spodoptera frugiperda* (Sf9) cells encoded on vectors listed in the key resources table. The culture conditions for expression of each protein are described in the STAR Methods section entitled "protein expression".

Please cite this article in press as: Pastok et al., Structural requirements for the specific binding of CRABP2 to cyclin D3, Structure (2024), https://doi.org/10.1016/j.str.2024.09.020

METHOD DETAILS

Protein expression

Human cellular retinoic acid-binding protein 2 (CRABP2, residues 1-138, UniProt entry P29373) and human CRABP1 (Uniprot entry P29762) were each cloned into pGEX-6P-1 (GE Healthcare) at *BamH*I and *EcoR*I restriction sites to generate a N-terminal glutathione-S-transferase (GST-tag) followed by a 3C protease recognition sequence using a synthesized DNA CRABP2 DNA template (Horizon Discovery) or a CRABP1 cDNA template.[7] N or C-terminal Avi-tag or CRABP2 point mutations were introduced using the QuikChange II Site-Directed Mutagenesis Kit (Agilent). Cloning and subsequent plasmid DNA preparation was carried out in *E. coli* DH5α. Forward primer sequences are provided in Table S2 and mutations are listed in the key resources table. Multisite mutants for which there are no primers listed were made by sequentially introducing mutations using the primers designed to introduce the single site mutations. All constructs were verified by sequencing. CRABP1-Avi, CRABP2 and CRABP2-Avi constructs were expressed in BL21STAR™ (DE3) (ThermoFisher Scientific) or Rosetta2 (DE3) pLYS-S (Novagen) *E. coli* cells grown at 30°C in 2xYT medium till OD_{600} of 0.7-0.8, cooled and then induced at 18°C by IPTG (0.5 mM) and further incubated for 16 h. The cells were harvested by centrifugation (4000 xg for 20 min at 4°C), resuspended in buffer (10 mM HEPES pH 7.5, 150 mM NaCl, 0.5 mM TCEP) supplemented with cOmplete EDTA-free protease inhibitor cocktail (Roche), 2 mg ml^{-1} DNAseI and 5 mM $MgCl_2$ and frozen prior to purification. Human p27 protein (1-106; Uniprot entry P46527) and p21 protein (1-87; Uniprot entry P38936) were cloned into pGEX-6P1 (GE Healthcare) at BamHI and EcoRI restriction sites as described previously in Hallett et al.[52] The proteins were expressed in BL21STAR™(DE3) *E. coli* and purified as described in Hallett et al.[52] Human CDK4 and CDK6 were expressed in *Sf*9 insect cells using a recombinant baculovirus expression system (Geneva-Biotech MultiBac™).[71] As described previously in Hallett et al.,[52] full length human CDK4 and CDK6 with an N-terminal glutathione-S-transferase (GST)-tag and 3C protease recognition site, were cloned separately into the pACEBac1 acceptor vector. Human untagged full-length cyclin D1 and cyclin D3 were cloned into the pIDK donor vector. Cre recombinase (New England Biolabs) was used in the Cre-LoxP reaction of acceptor and donor vectors to generate the multigene fusion for co-expression of CDK4 or CDK6 with either cyclin D1 or cyclin D3. All constructs were verified by restriction enzyme digestion and DNA sequencing. Approximately 5-10 ng of DNA vector pACE-BAC-1-CDK or an acceptor-donor fusion pACE-Bac-1-pIDK for CDK and cyclin D co-expression) was used to transform EmBacY *E. coli* cells harboring the EMBacY MultiBac™bacmid (for constitutive expression of yellow fluorescent protein YFP). DNA sequences of interest were transferred to the bacmid via transposition into the mini Tn7 attachment site. White recombinant colonies were selected for subsequent bacmid preparation. MultiBac bacmid DNA was prepared by alkaline lysis (QIAprep Miniprep kit (Qiagen)). The final supernatant was precipitated using isopropanol (40%) and the resulting pellet was then washed twice with 70% ethanol, dried and resuspended in sterilised water in sterile conditions. For the transfection reaction, transfection reagent (GeneJuice™ (Novagen)) was added to the resuspended bacmid DNA and the resulting cocktail was used to infect 0.5 x 10^6 *Sf*9 cells seeded in 6-well plates. After 48-60 h incubation at 27°C, the supernatant was collected, and positive transfection was verified by monitoring the appearance of yellow cells constitutively expressing the YFP gene and containing the constructs of interest by fluorescence microscopy. This initial virus stock (Vo) was amplified twice and then used for protein expression. Insect cells were harvested after 72 h of infection, resuspended in 10 mM HEPES pH 7.5, 150 mM NaCl, 0.5 mM TCEP (resuspension buffer) supplemented with a cOmplete EDTA-free protease inhibitor cocktail (Roche) and stored at -20°C. To produce cyclin D3 mutants, point mutations were introduced using the QuikChange II Site-Directed Mutagenesis Kit (Agilent) in the pIDK-cyclin D3 wild type construct. Cloning and subsequent plasmid DNA preparation was carried out in *E. coli* DH5α. All constructs were verified by sequencing. Once correct sequences for point mutations were confirmed, Cre-recombinase was used as for pIDK-cyclin D3 to generate multigene fusions for co-expression with CDK4 and CDK6 as for wild type protein. Procedure was repeated for baculovirus preparation. To produce complex CDK4-cyclin D3-p21, p21 (1-87) was cloned into pIDS donor vector. As above Cre recombinase (New England Biolabs) was used in the Cre-LoxP reaction of acceptor and donor vectors to generate the multigene fusion for co-expression of CDK4 with cyclin D3 and p21. All constructs were verified by restriction enzyme digestion and DNA sequencing. Procedure was repeated for baculovirus preparation.

Protein purification

GST-tagged proteins used in this study were purified as follows. Bacterial or insect cell pellets were thawed on ice and lysed by sonication (total of 5 min with 30% amplitude and pulsed for 20 s on and 40 s off). Lysates were subsequently cleared by centrifugation (100,000 xg at 4°C for 1hr). Supernatant was recovered and incubated with gentle rotation for 3 hr at 4°C with Glutathione Sepharose 4B resin (Cytiva), pre-equilibrated in loading buffer (10 mM HEPES pH 7.5, 150 mM NaCl and 0.5 mM TCEP). The resin was then loaded into a gravity flow column and washed with 50 mL of loading buffer. Bound protein was eluted in 1 ml fractions with loading buffer supplemented with 20 mM reduced glutathione and adjusted to pH 8.0. Fractions containing protein were combined and incubated overnight with 1:50 (w/w) 3C protease at 4°C. Cleaved protein was further purified by size exclusion chromatography using either a Superdex 75 or Superdex 200 HiLoad column (Cytiva) equilibrated in loading buffer. Fractions containing protein were pooled and reapplied to Glutathione Sepharose 4B resin to remove the GST and GST-3C protease. Flowthrough was collected and analysed by SDS-PAGE and visualised using Instant Blue stain (Expedeon). Protein concentrations were determined by NanoDrop2000 UV-Vis spectrophotometer (Thermo Scientific) and sequence estimated extinction coefficients. Proteins were concentrated to 5 mg ml^{-1}, flash frozen using liquid nitrogen and stored at -80°C.

Please cite this article in press as: Pastok et al., Structural requirements for the specific binding of CRABP2 to cyclin D3, Structure (2024), https://doi.org/10.1016/j.str.2024.09.020

Protein structure determination

CRABP2_R30D/K31D and CRABP2_R30A/K31A were concentrated to 10 mg ml^{-1} and 5 mg ml^{-1} respectively prior to setting up crystallization plates. Initial crystallization conditions were identified following screening against a wide range of commercially available screens using the sitting drop vapour diffusion method. Typically drops at 1:1 or 2:1 protein:well solution ratios (200 nl and 300 nl total drop and 100 μl well volumes) were set up using a Mosquito robot (SPT Labtech) and incubated at 20°C. Single crystals were identified in 100 mM $CH_3COONa \cdot 3H_2O$ pH 4.5 with 2.0 M $(NH_4)_2SO_4$ (CRABP2_R30D/K31D) and 150 mM $MgCl_2$, 100 mM Bis-Tris pH 6.5 and 25% PEG 3350 (CRABP2_R30A/K31A). Crystals were cryo-protected by a quick transfer in a saturated (~3.5 M) $(NH_4)_2SO_4$ solution (CRAPB2_R30D/K31D), or the reservoir solution was supplemented with 20% PEG 400 (CRABP2_R30A/K31A) and then flash cooled in liquid nitrogen before data collection. Data were collected at the Diamond Light Source (Oxfordshire, UK) on beamlines I03 (CRABP2_R30D/K31D) and I24 (CRABP2_R30A/K31A). Data was processed using XIA2/XDS,[72,73] POINTLESS/AIMLESS,[74,75] and other programs of the CCP4 suite,[76] run through the CCP4i2 GUI,[77] or CCP4 Cloud.[78] The CRABP2_R30A/K31A structure was solved by molecular replacement using Phaser[79] and the CRABP2_R30D/K31D structure was solved by molecular replacement using MOLREP[80,81] using PDB model 2FRS as the search model in both cases. The structures were refined using cycles of automated refinement in REFMAC[82] and manual model building in Coot.[83] The models were validated using Coot[83] and Molprobity[84] validation tools. The statistics of the data sets and the crystallographic refinement are presented in Table 2. The structures and their associated structure factors have been deposited in the PDB with accession codes 7OXX and 7OXW for CRABP2_R30D/K31D and CRABP2_R30A/K31A respectively. Electron density figures were prepared using ChimeraX.[85]

Retinoid binding assay

Retinoid derivative DC271 was dissolved in <1% ethanol to 150, 125, 100, 75, 50, 25,12.5, 6.25 nM) and CRABP2 (wild-type and mutants) was diluted to 100 nM in 20 mM K_2HPO_4, 100 mM KCl, pH 7.4, 0.05% Pluronic F127. 50 μl CRABP2 solution or a buffer control was dispensed into a Corning, black Non-binding Surface (NBS) 96 well plate cleaned using compressed air and then titrated against 50 μl of the DC271 dilution series (total well volume 100 μl). Plates were then spun at 460 xg for 2 min to ensure mixing. Fluorescence was measured using a Synergy H4 plate reader, at excitation/emission wavelengths of 355/460 nm respectively. Technical replicates were performed using protein from the same source. Data were plot and analysed in PRISM (GraphPad).

CRABP1 and CRABP2 biotinylation

As the extent of CRABP1/2 biotinylation by *E. coli* BirA activity during protein expression was <5%, CRABP1/2 (wild-type and mutants) were further modified by incubating 40 μM of the purified Avi-tagged protein with 10 μg BirA in biotinylation buffer (50 mM Bicine pH 8.3, 10 mM ATP, 10 mM MgOAc, 50 μM *d*-biotin) at 30°C for 30 minutes. Protein was then buffer exchanged using size exclusion chromatography into HTRF buffer A (50 mM HEPES pH 7.5, 100 mM NaCl). The extent of protein biotinylation was monitored by mass spectrometry.

Homogenous time-resolved fluorescence (HTRF)

Direct binding format

In the direct binding assay format GST-tagged cyclin-dependent kinase 4 or 6 (CDK4/6) or bound to cyclin D1 or cyclin D3 (GSTCDK) was incubated with biotinylated Avi-tagged protein of interest (CRABP1, CRABP2 or p27 residues 1-106 ($p27_{1-106}$)) to form a GSTCDK-protein complex. The complex was then incubated with a Tb-labelled anti-GST antibody and streptavidin-tagged XL665 dye. Formation of a complex brings the Tb and XL665 into proximity so that excitation of the Tb results in emission from the XL665 dye as a result of Förster resonance energy transfer (FRET) between the two probes. For direct binding measurements the biotinylated protein of interest was initially titrated, over 11 serial dilution points and an additional buffer blank point, against 10 nM of either GSTCDK4 or GSTCDK6. Concentrations of GSTCDK and the binding protein of interest were prepared in HTRF buffer A (50 mM HEPES, 100 mM NaCl, 1 mM DTT and 0.1 mg ml^{-1} BSA) and incubated together for 60 min at 4°C. 5 nM Tb labelled anti-GST antibody and SAXL665 at 1/8th the concentration of the biotinylated protein, were prepared in HTRF buffer B (50 mM HEPES, 100 mM NaCl and 0.1 mg ml^{-1} BSA) and added to each well. The plate was incubated for a further 120 min at 4°C, before being scanned. Samples were excited using a wavelength of 337 nm and emission spectra measured at 620 nm and 665 nm (PHERAstar FS (BMG LABTECH)). Binding curves were plotted using GraphPad Prism 6 from which the K_ds were determined. The curves shown are representative binding curves from at least two runs carried out on separate days.

Competition mode

10 nM GSTCDK4 or GSTCDK6 and 118 nM N-Avi CRABP2 (the CRABP2 concentration was adjusted to the measured K_d for the CDK-CRABP2 interaction), were added to each well along with a serial dilution of the competitor (either RA derivatives, or CRABP2 mutants). All dilutions were made using HTRF buffer A (50 mM HEPES, 100 mM NaCl, 1 mM DTT and 0.1 mg ml^{-1} BSA) and set up in duplicate. RA derivatives stocks were prepared in 100% ethanol. The plate was incubated for 60 min at 4°C, before 5 nM Tb labelled anti-GST antibody and 14.75 nM of SAXL665 (for both the CDK4 and CDK6 measurements) were added to each well. Concentrations of the Tb antibody and SAXL665 were made up using HTRF buffer B (50 mM HEPES, 100 mM NaCl and 0.1 mg ml^{-1} BSA). The plate was incubated for a further 120 min at 4°C, before being scanned. Samples were excited using a wavelength of 337 nm and emission spectra measured at 620 nm and 665 nm (PHERAstar FS (BMG LABTECH)). Percentage inhibition graphs were plotted using GraphPad Prism 6, by comparing to a maximum signal, where no competitor is present, and a minimum signal, where no GSTCDK4 or GSTCDK6 is present.

Please cite this article in press as: Pastok et al., Structural requirements for the specific binding of CRABP2 to cyclin D3, Structure (2024), https://doi.org/10.1016/j.str.2024.09.020

Analytical size exclusion chromatography

CDK6-cyclin D3 and CRABP2 were incubated on ice for 60 min at a molar ratio of 1:2 and analyzed on a Superdex200 10/30 column (Cytiva) pre-equilibrated in 10 mM HEPES pH 7.5, 50 mM NaCl, 0.5 mM TCEP at 4°C. To assess CRABP2_R30A_K31A and CRABP2_R30D_K31D solution properties 20 μM of each protein was analyzed on a Superdex 75 10/30 column (Cytiva) pre-equilibrated in 10 mM HEPES pH 7.5, 150 mM NaCl, 0.5 mM TCEP at 4°C. The experiment included determination of a standard curve run under the same conditions.

Protein complex detection by pulldown

50ml *Sf*9 cell cultures (1x10^6 cells per ml) were infected with GSTCDK6-cyclin D3 (WT and cyclin D3 mutants) baculovirus (1:50) and incubated for 72 h at 27°C, 120 rpm. Cultures were harvested at 4000 xg for 10 min and the supernatant discarded. Pellets were snap frozen, thawed, and resuspended in 10 mM HEPES pH 7.5, 100 mM NaCl, 0.5 mM TCEP, 1% Tween-20. Lysates were centrifuged at 20000 xg for 20 min at 4°C. The supernatant was mixed with 100 μL Glutathione Sepharose 4B (Cytiva, 17075601), pre-equilibrated with 10 mM HEPES pH 7.5, 100 mM NaCl, 0.5 mM TCEP, for 1 h at 4°C, with gentle agitation. GSTCDK6-cyclin D3 bound Glutathione Sepharose was centrifuged (500 xg 2 min) the supernatant discarded and the sepharose washed with 10 mM HEPES pH 7.5, 100 mM NaCl, 0.5 mM TCEP. Once washed, the sepharose was split and incubated with purified CRABP2 (~10 μM) or p27 1-106 (~15 μM) at 4°C for 2 h. The sepharose was harvested and unbound fraction collected. The sepharose was washed and resuspended in 30 μL of 5x Sample Buffer (Genscript, MB01015) to elute the complex. Unbound samples and bound samples were analysed by SDS-PAGE. Each set of pull down experiments was carried out using two independently prepared samples of CDK6-cyclin D3 and repeated three times. The samples of CRABP2 and p27 were each from the same purification, but different stock aliquots.

Structural analysis of iLBP family members

Amino acid sequences were retrieved from the UniProt database (www.uniprot.org, The UniProt Consortium).[86] Alignments were performed using Clustal Omega[87] and visualised using Jalview.[88] The alignments were rendered using ESPript3.0 (http://espript.ibcp.fr).[89] All figures of structures were plotted in Chimera UCSF[90] or ChimeraX.[85]

Molecular dynamics simulations

The crystal structure of apo CRABP2 (PDB: 2FS7) was retrieved from the Protein Data Bank (PDB); additional chains and all solvent molecules were removed. The DockPrep tool of UCSF Chimera[90] was used to complete missing/incomplete side chains. This model was used as 'WT-OPEN' for CRABP2. The 'WT-COLLAPSED' model of CRABP2 was derived from the CRABP2_R30D_K31D mutant structure which was prepared as above and the UCSF Chimera rotamers tool used to revert the 30/31 mutations to wild-type. Protein models were simulated in GROMACS 2020.2[60] using the AMBER99SB forcefield[91] in a 10 Å shell cubic box (66 x 66 x 66 Å) with TIP3P water and charges neutralized to 0.1 M NaCl. Steepest descent energy minimization of maximum 5000 steps was used to prepare structures for subsequent simulation in triplicate with randomly assigned, independent velocities. Position restraints were used for 200 ps equilibration in the NvT ensemble using a 2 fs timestep and Nose-Hoover temperature coupling at 300 K, followed by equilibration in the NpT ensemble under position restraints with Parinello-Rahman barostat at 1 bar. Finally, position restraints were released for 400 ns production MD. All analysis was carried out using GROMACS packages and presented using GraphPad Prism 8 and custom script using Python modules including NumPy.[92]

AlphaFold Multimer modelling

Alphafold2 Multimer was accessed via ColabFold74 (v1.3) and used to predict the binding of CRABP2 to CDK6-cyclin D1/2/3 complexes. Single amino acid protein sequences for CDK4/6-cyclin D3 and CRABP2 were inputted with ":" to specify inter-protein chain breaks for modelling complexes. AlphaFold Multimer was subsequently run with default settings: 5 models generated with 3 recycles per model.

AlphaFold Multimer sub-sampling

The sequence of full length CRABP2 (wild type) was supplied to the sub-sample implementation on Colab[61] v1.0.1 and used to probe varying *maxseq:extraseq* ratios using up to 5 independent seeds (total 1000 PDBs) and default settings. Output DCD trajectories for each ratio were compiled and converted to GROMACS XTC format using MDAnalysis 2.7.0.[93] Open and closed reference conformations were drawn from the 2:8 sample population as close structural matches for the crystal structures. RMSDs for each structure within the conformational ensemble predicted were then calculated by least squares alignment of each trajectory frame (1000 frames total) Cα backbone to reference conformations, with output for residues 15-38 (α1-loop-α2 helical cap region), using gmx rms within GROMACS.

QUANTIFICATION AND STATISTICAL ANALYSIS

Retinoid binding assay

Technical replicates were performed using protein from the same source. Details are included in the legend to Figure S2. Data were plot and analysed in PRISM (GraphPad Software, San Diego, CA, USA).

Please cite this article in press as: Pastok et al., Structural requirements for the specific binding of CRABP2 to cyclin D3, Structure (2024), https://doi.org/10.1016/j.str.2024.09.020

CellPress
OPEN ACCESS

Homogenous time-resolved fluorescence

Measurements were carried out in duplicate and repeated on 3 separate days. The error bars indicate SD. Replicate details for each experiment are included in the legends to Figures 1, 2, 5, S1, S2, and S7. Direct binding curves were plotted using GraphPad Prism 6. Percentage inhibition graphs were plotted using GraphPad Prism 6, by comparing to a maximum signal, where no competitor is present, and a minimum signal, where no GSTCDK4 or GSTCDK6 is present. CRABP2 mutant effects on CDK4/6-cyclin D3 binding were assessed by Kruskal-Wallis tests in comparison to wild type CRABP2 binding.

Analytical size exclusion chromatography

Analysis was carried out in replicate using independently prepared proteins.

Protein complex determination by pulldown

Each set of pull down experiments was carried out using two independently prepared samples of CDK6-cyclin D3 and repeated three times. The samples of CRABP2 and p27 were each from the same purification, but different stock aliquots. Details are included in Figures 5 and S7 legends.

Molecular dynamics simulations

Simulations of each system were performed in triplicate. Each simulation was analysed independently using GROMACS packages. Details are included in Figure S5. RMSD and RMSF values for triplicate simulations were plotted as range and mean in Graphpad Prism 8, presented in Figure 4.

AlphaFold Multimer modelling

Each complex within the matrix of CDK4/6-cyclin D-CRABP proteins was run once to produce 5 models; representative examples of package-generated graphs for sequence coverage and prediction quality (pIDDT) are given in Figure S6. The Predicted Aligned Error graphs generated by AlphaFold Multimer for each of the top scoring models was used to present the matrix in Figure S6A.

AlphaFold Multimer sub-sampling

The MDAnalysis package was used to convert the output DCD trajectories from AlphaFold Multimer Sub-Sampling to a GROMACS-readable XTC trajectory. GROMACS packages were used to compare RMSDs of each conformation to a reference model of the open and closed CRABP2 conformations. Graphs for Figure S5C were plotted in Microsoft Excel.

X-ray data collection and analysis

X-ray crystallography data collection and refinement statistics are summarized in Table 2.